ORIGINAL RESEARCH

Spontaneous Pancreatitis Caused by Tissue-Specific Gene Ablation of *Hhex* in Mice

Mark J. Ferreira,[1] Lindsay B. McKenna,[1] Jia Zhang,[1] Maximilian Reichert,[2] Basil Bakir,[2] Elizabeth L. Buza,[3] Emma E. Furth,[4] Clifford W. Bogue,[5] Anil K. Rustgi,[2] and Klaus H. Kaestner[1]

[1]Department of Genetics and Institute for Diabetes, Obesity, and Metabolism, Perelman School of Medicine, University of Pennsylvania, Philadelphia, Pennsylvania; [2]Division of Gastroenterology, Department of Medicine, Abramson Cancer Center, Perelman School of Medicine, University of Pennsylvania, Philadelphia, Pennsylvania; [3]Department of Pathobiology, School of Veterinary Medicine, University of Pennsylvania, Philadelphia, Pennsylvania; [4]Department of Pathology and Laboratory Medicine, Perelman School of Medicine, University of Pennsylvania, Philadelphia, Pennsylvania; [5]Department of Pediatrics, Yale University School of Medicine, New Haven, Connecticut

SUMMARY

Hhex is expressed in developing and mature pancreatic ductal cells. Embryonic *Hhex* ablation leads to chronic pancreatitis, yet Hhex is not required for mature exocrine compartment maintenance. Hhex represses G-protein coupled receptor *Npr3*, and thus likely ductal cell secretion.

BACKGROUND & AIMS: Perturbations in pancreatic ductal bicarbonate secretion cause chronic pancreatitis. The physiologic mechanism of ductal secretion is known, but its transcriptional control is not. We determine the role of the transcription factor hematopoietically expressed homeobox protein (*Hhex*) in ductal secretion and pancreatitis.

METHODS: We derived mice with pancreas-specific, Cre-mediated *Hhex* gene ablation to determine the requirement of Hhex in the pancreatic duct in early life and in adult stages. Histologic and immunostaining analyses were used to detect the presence of pathology. Pancreatic primary ductal cells were isolated to discover differentially expressed transcripts upon acute *Hhex* ablation on a cell autonomous level.

RESULTS: Hhex protein was detected throughout the embryonic and adult ductal trees. Ablation of *Hhex* in pancreatic progenitors resulted in postnatal ductal ectasia associated with acinar-to-ductal metaplasia, a progressive phenotype that ultimately resulted in chronic pancreatitis. *Hhex* ablation in adult mice, however, did not cause any detectable pathology. Ductal ectasia in young mice did not result from perturbation of expression of Hnf6, Hnf1β, or the primary cilia genes. RNA-seq analysis of *Hhex*-ablated pancreatic primary ductal cells showed mRNA levels of the G-protein coupled receptor natriuretic peptide receptor 3 (*Npr3*), implicated in paracrine signaling, up-regulated by 4.70-fold.

CONCLUSIONS: Although Hhex is dispensable for ductal cell function in the adult, ablation of *Hhex* in pancreatic progenitors results in pancreatitis. Our data highlight the critical role of *Hhex* in maintaining ductal homeostasis in early life and support ductal hypersecretion as a novel etiology of pediatric chronic pancreatitis. *(Cell Mol Gastroenterol Hepatol 2015;1:550–569; http://dx.doi.org/10.1016/j.jcmgh.2015.06.007)*

The exocrine pancreas, composed of acinar and ductal cells, plays a crucial role in digestion by delivering alkaline, isotonic pancreatic juice containing digestive enzymes to the duodenum. Pancreatic zymogens, released from acini in response to postprandial enterohormonal and neural signals, traverse an intricate network of ducts of increasing size.[1–3] Rather than merely serving as conduits, the pancreatic ducts actively aid in digestion by secreting bicarbonate against an immense concentration gradient.[4] Similar to acinar cells, ductal cells are stimulated to secrete in response to enterohormonal and neural inputs via the cyclic adenosine 5′-monophosphate/protein kinase A and calcium/phospholipase C-β signaling pathways.[5–9] Additionally, various paracrine factors released from acinar cells have been identified that augment ductal cell stimulation, ensuring a coordinated pancreatic response.[10,11]

Bicarbonate secretion serves to solubilize intraluminal zymogens and neutralize acidic chyme in the duodenum.[12] Impairment of ductal cell functioning, such as what is

Ⓜ **Most current article**

frequently observed in patients harboring mutations in the cystic fibrosis transmembrane conductance regulator (CFTR), contributes to the pathogenesis of pancreatic insufficiency and chronic pancreatitis, an important risk factor for pancreatic ductal adenocarcinoma.[13–15] Although the mechanism by which bicarbonate is transported across the pancreatic ductal epithelium has been elucidated, the transcriptional control governing this process remains poorly understood.

Recently, we reported that the transcription factor Hhex (hematopoietically-expressed homeobox protein), initially described as Prh (proline-rich homeodomain) in chicken, is expressed in the pancreatic ductal epithelium;[16,17] however, its function in this cell type and its potential contribution to pancreatic disease pathogenesis have not been determined. Previous studies indicate that Hhex is critical for proper development of structures derived from all three germ layers, including liver, thyroid, forebrain, heart, hematopoietic progenitors, and endothelium.[18–20] In the endoderm, *Hhex* is first expressed throughout the primitive endoderm but is later restricted to the visceral endoderm before gastrulation.[21,22] At embryonic development day 7 (E7.0), *Hhex* transcripts are localized to the anterior endoderm and the ventral-lateral foregut, the site of ventral pancreatic and liver organogenesis. *Hhex* mRNA is expressed at E10.0 in precursors of the thymus, liver, thyroid, dorsal pancreatic bud, and gallbladder.[23] By E13.5, endodermal *Hhex* expression is limited to the thyroid, liver, epithelial cells of the pancreas and extrahepatic biliary ducts, and most cell types of the lung, and it is notably high in the epithelia of the extrahepatic bile ducts and pancreas at E16.5.[23] In the adult mouse, Hhex gene activity has been previously described in the lung, thyroid, and liver;[23] moreover, Hhex has been shown to regulate directly functional genes in various mature cell types, such as somatostatin in δ-cells.[17]

The expression pattern of Hhex in the ventral-lateral foregut prior to pancreas specification suggests that it may serve an essential function in pancreatic development. Indeed, $Hhex^{-/-}$ mice fail to specify the ventral pancreatic bud, and they exhibit variable forebrain truncation, thyroid hypoplasia, and cannot expand the hepatic primordium.[20,24,25] Importantly, the failure of ventral pancreatic morphogenesis was determined to be the result of lack of proliferation of the definitive endoderm, thus compromising cell migration and subjecting these cells to morphogenetic inhibition by signaling from the cardiac mesoderm.[24] This cell-extrinsic mechanism was confirmed by the proper induction of the pancreatic progenitor gene *Pdx1* and the proendocrine genes *Isl1*, *Ngn3*, and *NeuroD* when $Hhex^{-/-}$ endodermal explants were grown away from the cardiac mesoderm.[24] Embryonic lethality of $Hhex^{-/-}$ mice, however, precluded any further analysis of the role of Hhex in pancreatic development or function.

Here, we characterized the expression dynamics of Hhex within the ductal compartment of the pancreas and determined its requirement for ductal development and function by employing conditional gene ablation in mice. Ablation of *Hhex* in pancreatic progenitors resulted in postnatal ductal ectasia that progressed to chronic pancreatitis later in life,

Table 1. Primers Used for Genotyping Analysis

Primer	Sequence (5′→3′)	Product Size (bp)
Hhex-F	ATTGACGGAAATGTTGCCATA	WT: 473
Hhex-R	CCAAGTGACACGATCCAGAAC	loxP: 605
CreERT2-F	TTTCAATACCGGAGATCATGC	550
CreERT2-R	ATTCCTGTCCAGGAGCAAGTT	
Cre-F	GCGGCATGGTGCAAGTTGAAT	232
Cre-R	CGTTCACCGGCATCAACGTTT	
YFP1	AAGACCGCGAAGAGTTTGTC	WT: 600
YFP2	GGAGCGGGAGAAATGGATATG	YFP+: 320
YFP3	AAAGTCGCTCTGAGTTGTTAT	

consistent with a published model of ductal hypertension.[26] Moreover, we identified the G-protein coupled receptor natriuretic peptide receptor 3 (*Npr3*), the activation of which is reported to potentiate secretin signaling to increase pancreatic flow rate, as regulated by Hhex and likely contributing to the pathogenesis of chronic pancreatitis in this genetic model.[27]

Materials and Methods

Mice

The derivation of the $Hhex^{loxP}$ allele has been described previously elsewhere.[28] *Pdx1-Cre^{Early}* mice were kindly provided by Dr. Guoqiang Gu and Dr. Doug Melton, and *Sox9-CreER^{T2}* mice were kindly provided by Dr. Maike Sander.[29,30] The mice were maintained on a 129SvEv/C57BL/6 mixed background. Genotyping was performed by polymerase chain reaction (PCR) analysis using genomic DNA isolated from toe snips of newborn mice. The genotyping primers are provided in Table 1, and the thermocycler conditions were as follows: $Hhex^{loxP}$ and $CreER^{T2}$: 94°C for 4 minutes [94°C for 35 seconds, 60°C for 35 seconds, 72°C for 50 seconds] 33 times, 72°C for 7 minutes, 4°C indefinitely; *Cre*: 94°C for 5 minutes [94°C for 30 seconds, 56°C for 45 seconds, 72°C for 60 seconds] 30 times, 72°C for 10 minutes, 4°C indefinitely; and *YFP*: 94°C for 3 minutes, [94°C for 30 seconds, 50°C for 60 seconds, 72°C for 60 seconds] 35 times, 72°C for 2 minutes, 4°C indefinitely. Experimental mice were derived from crossing $Hhex^{loxP/loxP}$ animals with either $Hhex^{loxP/loxP};Pdx1-Cre^{Early}$ or $Hhex^{loxP/loxP};Sox9-CreER^{T2}$ mice; $Hhex^{loxP/loxP}$ littermates were used as controls for all experiments. For timed matings, the morning at which a vaginal plug was present was considered day E0.5.

For experiments with tamoxifen induction, adult mice (>9 weeks of age) were administered 5 mg of tamoxifen (T5648, Lot SLBF8049V; Sigma-Aldrich, St. Louis, MO) per 40 g of body mass for 3 consecutive days by oral gavage. Tamoxifen was suspended in a 10% ethanol/90% sunflower seed oil (S5007; Sigma-Aldrich) (v/v) mixture at 20 mg/mL and rotated at 42°C for 2 hours until completely dissolved. All procedures involving mice were approved by the University of Pennsylvania Institutional Animal Care and Use Committee.

Histologic Analysis

For studies with adult mice, pancreata were dissected and fixed in 4% paraformaldehyde/phosphate-buffered saline (PBS) (w/v) for 16 hours at 4°C, followed by three 10-minute washes with 1x PBS. Pancreata were laid flat in tissue cassettes for paraffin embedding. The fixation times for embryonic/perinatal mice were adjusted as follows: E13.5–E18.5, 1 hour; postnatal day 3 (P3), 2 hours; P10, 4 hours; and P21, 10 hours. Paraffin sections with the maximal footprint were used for all experiments.

For all histologic studies, slides were dewaxed/rehydrated in a xylene-ethanol series, followed by antigen retrieval in citric acid buffer pH 6.0 in a 2100 Classic Clinical Autoclave (Prestige Medical) if needed (Table 2). After 2 hours of cooling, slides were rinsed for 10 minutes in running tap water. For immunohistochemistry, endogenous peroxidase activity was blocked by placing slides in 3% hydrogen peroxide for 15 minutes, followed by a 5-minute wash in water. Slides were then blocked with avidin D and biotin blocking reagents (SP-2001; Vector Laboratories, Burlingame, CA) for 15 minutes each at room temperature, with a quick rinse of PBS in between. Slides were blocked with CAS-Block (008120; Invitrogen/Life Technologies, Carlsbad, CA) for 30 minutes at room temperature.

Primary antibodies (see Table 2) were diluted in CAS-Block and incubated overnight at 4°C, followed by species-specific biotinylated secondary antibody (see Table 2; 1:200 in PBS/0.1% Triton X-100) incubation for 40 minutes at 37°C. Signals were developed using the Vectastain Elite ABC Kit (PK-6100; Vector Laboratories) and peroxidase substrate 3,3′-diaminobenzidine (DAB) Kit (SK-4100; Vector Laboratories) according to the manufacturer's instructions.

For immunofluorescence, the slides were blocked with CAS-Block for 30 minutes at room temperature after antigen retrieval and then incubated with primary antibody (see Table 2) diluted in CAS-Block overnight at 4°C, followed by species-specific fluorescently conjugated secondary antibody (see Table 2; 1:500 in CAS-Block) for 2 to 4 hours at room temperature. The slides were mounted with fluorescent mounting medium (71-00-16; KPL, Gaithersburg, MD) or Vectashield mounting medium with 4,6-diamidino-2-phenylindole (DAPI, H-1200; Vector Laboratories). All histologic images were obtained using a Nikon Eclipse 80i microscope (Nikon, Tokyo, Japan) with a Q-imaging Retiga

Table 2. Primary and Secondary Antibodies Used for Immunostaining Analysis

Primary Antisera

Antigen	Species	Dilution	Antigen Retrieval	Source	Lot No.
Ac-Tub	Mouse	1:1000	Yes	Sigma-Aldrich (T7451)	103M4772V
GFP	Goat	1:500	Yes	Abcam (ab6673)	10
Hhex	Rabbit	1:250	Yes	Dr. Clifford Bogue[75]	
Hnf1β	Goat	1:100	Yes	Santa Cruz (sc-7411)	E1010
Hnf6	Guinea Pig	1:1000	Yes	Kind gift from Dr. Patrick Jacquemin[40]	
Muc1	Armenian Hamster	1:200	Yes	NeoMarkers (MAbHM-1630-P1Abx)	1630X1210A
Ngn3	Guinea Pig	1:1000	Yes	Kind gift from Dr. Maike Sander	
Npr3	Rabbit	1:50	No	Thermo Scientific (PA5-22080)	PH1894881J
Phospho-p38	Mouse	1:200	Yes	Santa Cruz (sc-7973)	H2007
SMA	Rabbit	1:200	Yes	Abcam (ab5694)	GR110346-1
Sox9	Goat	1:100	Yes	Santa Cruz (sc-17340)	L0408

Secondary Antisera

Raised against	Raised in	Conjugate	Dilution	Source
Goat IgG	Horse	Biotin	1:200	Vector Laboratories (BA-9500)
Guinea Pig IgG	Goat	Biotin	1:200	Vector Laboratories (BA-7000)
Mouse IgG	Goat	Biotin	1:200	Vector Laboratories (BA-9200)
Rabbit IgG	Goat	Biotin	1:200	Vector Laboratories (BA-1000)
Rabbit IgG	Donkey	Cy3	1:500	Jackson ImmunoResearch (711-165-152)
Armenian Hamster IgG	Goat	Cy2	1:500	Jackson ImmunoResearch (127-225-160)
Armenian Hamster IgG	Goat	Cy3	1:500	Jackson ImmunoResearch (127-165-160)
Mouse IgG	Goat	Cy2	1:500	Jackson ImmunoResearch (115-225-166)
Mouse IgG	Goat	Cy3	1:500	Jackson ImmunoResearch (115-165-166)
Guinea Pig IgG	Donkey	Cy2	1:500	Jackson ImmunoResearch (706-485-148)
Goat IgG	Bovine	Cy2	1:500	Jackson ImmunoResearch (805-545-180)
Goat IgG	Bovine	Cy5	1:500	Jackson ImmunoResearch (805-605-180)

Table 3. Primers Used for Gene Expression Analysis by Quantitative Reverse-Transcription Time Polymerase Chain Reaction

Transcript	Forward Primer Sequence (5′→3′)	Reverse Primer Sequence (5′→3′)
Cys1	AAAGGCAACCCTGAAGACAG	GCCATGAGCTCCTCTTCTGA
Hhex	TCAGAATCGCCGAGCTAAAT	CTGTCCAACGCATCCTTTTT
Hnf1β	CATCTGCAATGGTGGTCACAG	GGCTTGCAGTGGACACTGTTT
Hnf6	CAAATCACCATCTCCCAGCAG	CAGACTCCTCCTCCTGGCATT
Kif3a	GAGAAGGGACCAAGCAGGTAAA	TCCTCGTCAATTTTCGCTTGC
Npr3	GCAAATCATCAGGTGGCCTA	CCATTAGCAAGCCAGCACCTA
Pkd1	CAAGGAGTTCCGCCACAAAG	AACTGGGGATGACTTGGAGC
Pkd2	CTGGATGTTGTGATTGTCGTGT	TAGCAGCCCCTCTGCATTTG
Pkhd1	AAGTCAAGGGCCATCACATC	ATGTTTCTGGTCAACAGCCC
Polaris	AACAGCGCATAAAATCGGGC	GGCACTCAGTCGTTCACTCT
Prkcsh	CCACAGAGGATGAGAAGATGC	TTTCAAGGACCGTTCGACTT
Sec63	GCTCTTCTGGAGACCAAGTCA	AAAGCCACCACCACTCTTGT
Sst	CCCAGACTCCGTCAGTTTCT	GGGCATCATTCTCTGTCTGG
Tbp	CCCCTTGTACCCTTCACCAAT	GAAGCTGCGGTACAATTCCAG

2000R camera (QImaging, Surrey, BC, Canada) using iVision software (BioVision Research, Mountain View, CA). The numerical apertures of the objectives were as follows (mag/NA): 4×/0.13, 10×/0.30, 20×/0.50, 40×/0.75.

To determine the presence of pathology, a veterinary anatomic pathologist assessed the histologic slides in a blinded manner. For measurement of duct diameter, slides were scanned, and all luminal diameters present on the pancreatic footprint were measured; data are presented as the mean of the average diameter of each animal for each genotype. For luminal contents score, a pathologist assigned each animal a single score in a blinded manner on a scale of 0–10, with 0 representing no luminal contents on average and 10 representing virtually all ducts completely occluded by inspissated, eosinophilic contents; data are presented as the mean score of each genotype.

Cell Counting and Morphometry

To determine the ablation efficiency of *Hhex* in each genetic model, >1000 ductal cells surrounding a lumen from at least four mutant pancreata were scored as Hhex$^+$
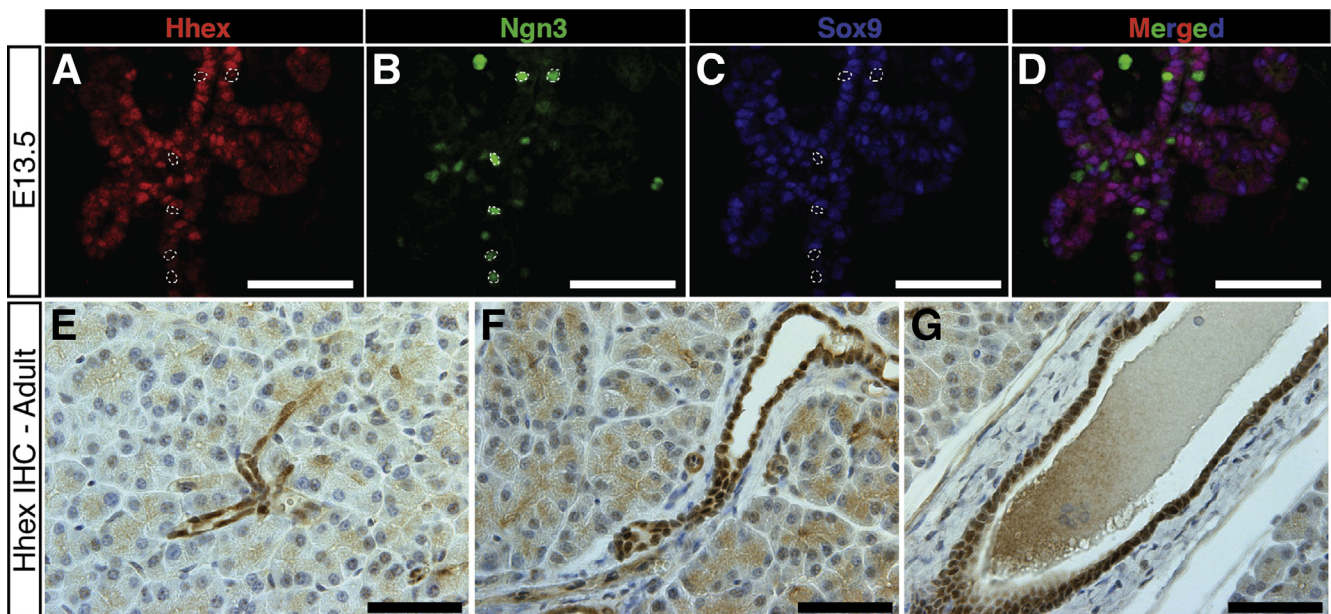

Figure 1. Hhex is expressed throughout embryonic and mature ducts. (*A–D*) Hhex (*A, D, red*) is expressed in the Sox9$^+$ (*C, D, blue*) pancreatic epithelium at E13.5, yet excluded from Ngn3$^+$ endocrine progenitors (*B, D, green*). Several Ngn3$^+$ cells are outlined (*A–C*). (*E–G*) Immunohistochemical staining for Hhex expression (*brown*) in the adult pancreas: (*E*) intercalated duct, (*F*) intralobular duct, (*G*) interlobar/main duct. Scale bars: 50 μm.
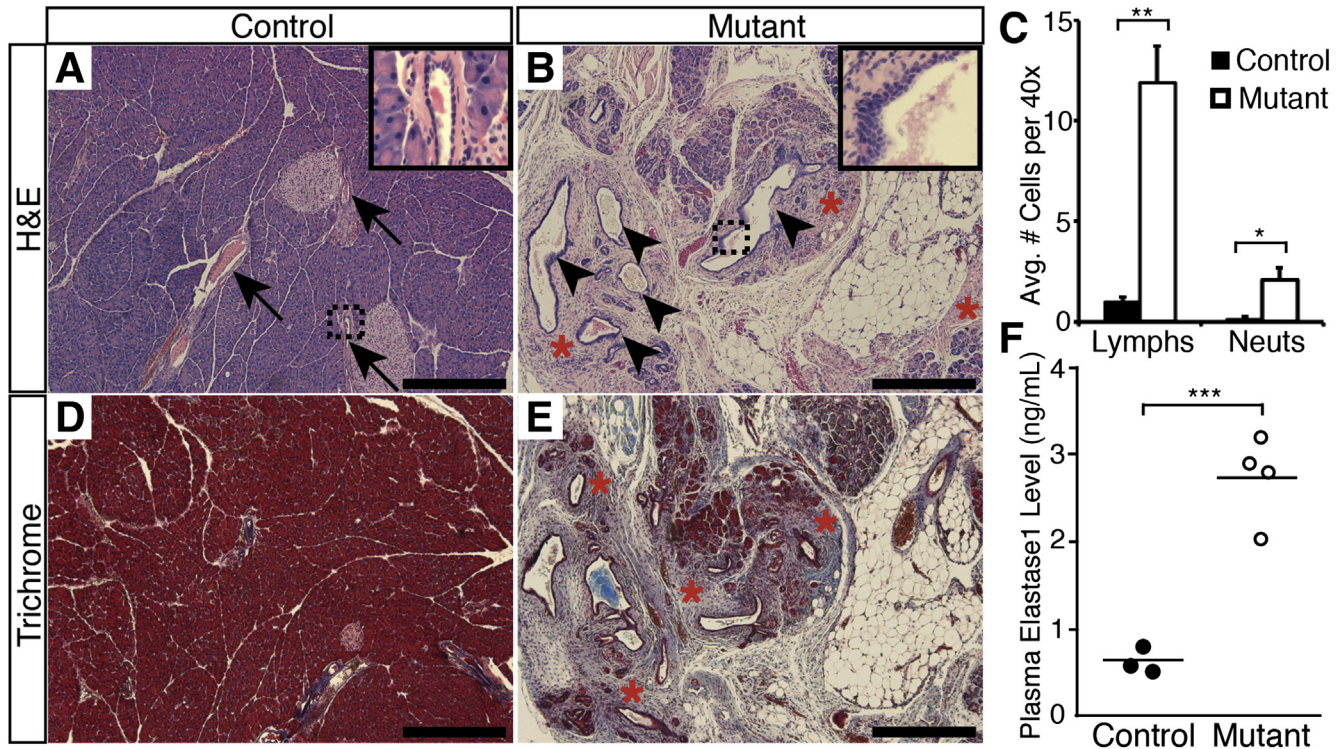
Figure 2. Ablation of *Hhex* in pancreatic progenitors results in chronic pancreatitis. (*A, B*) Representative H&E images of 18-week-old control (*Hhex^{loxP/loxP}*) and mutant (*Hhex^{loxP/loxP};Pdx1-Cre^{Early}*) pancreata (n = 3). (*A*) Ducts of control pancreata (*arrows*) are of typical caliber and consist of simple cuboidal epithelium (*inset*). (*B*) Mutant ducts display tortuous, ectatic ducts (*arrowheads* and *inset*) with parenchymal fibrosis (*red asterisks*). (*C*) Average numbers of lymphocytes and neutrophils were quantified from 20 random 40× fields (per animal) of control (*Hhex^{loxP/loxP}*, n = 3) and mutant (*Hhex^{loxP/loxP};Pdx1-Cre^{Early}*, n = 3) pancreata based on cell morphology. Mutant pancreata averaged 11.9 lymphocytes and 2.1 neutrophils per field, compared with 1.0 and 0.15, respectively, in controls. (*D, E*) Trichrome staining highlights periductal and interstitial fibrosis in mutant pancreata (*red asterisks*). (*F*) Measurement of plasma elastase-1 levels by enzyme-linked immunosorbent assay indicate an approximate 4.2-fold elevation in 8-week-old mutants (n = 4, mean 2.8 ng/mL) compared with age-matched controls (n = 3, mean 0.65 ng/mL). Mean of each group is indicated. Scale bars: 400 μm; *$P < .05$, **$P < .01$, ***$P < .001$, Student *t* test. *Insets*: magnification, 400×.

or Hhex⁻ based on immunohistochemical staining for Hhex. For lymphocyte and neutrophil quantification, 20 random H&E fields (magnification, 40×) from three animals of each genotype were scored for the presence of these cell types based on well-established morphologic criteria, and cells within the vasculature, ductal lumina, or intrapancreatic lymph nodes were excluded. Smooth muscle actin positive (SMA⁺) cells were quantified by scoring 20 random fields (magnification, 20×) of SMA-immunostained sections from three animals of each genotype. Data for neutrophil, lymphocyte, and SMA⁺ cell number are presented as average number per field.

To detect fibrillar collagens and quantify fibrosis, sections from P21 pancreata were stained with Sirius Red (90461; Chondrex, Redmond, WA) according to the manufacturer's instructions. Morphometric analysis was used to determine the percentage area that was positive for Sirius Red relative to the total pancreatic area as previously described elsewhere, with the exception of using two sections per mouse spaced >100 μm apart.[17] Each data point represents the average relative Sirius Red-positive area for each animal.

Elastase-1 Enzyme-Linked Immunosorbent Assay

Approximately 220 μL of blood was collected from the tail vein of each mouse using heparinized blood collecting tubes (02-668-10; Thermo Fisher Scientific, Waltham, MA). After centrifugation in plasma separator tubes with lithium heparin (365958; BD Biosciences, San Jose, CA), plasma was diluted 1:1 with PBS, and 100 μL was used per well in the elastase-1, Pancreatic (ELA1) BioAssay enzyme-linked immunosorbent assay kit (mouse) according to the manufacturer's instructions (024760; United States Biological, Salem, MA). The assay was performed in technical duplicate for each animal. Absorbance at 450 nm was measured using a Multiskan FC Microplate Photometer (51119000; Thermo Fisher Scientific).

RNA Extraction, Quantitative Reverse-Transcriptase Polymerase Chain Reaction, and Transcriptome Analysis

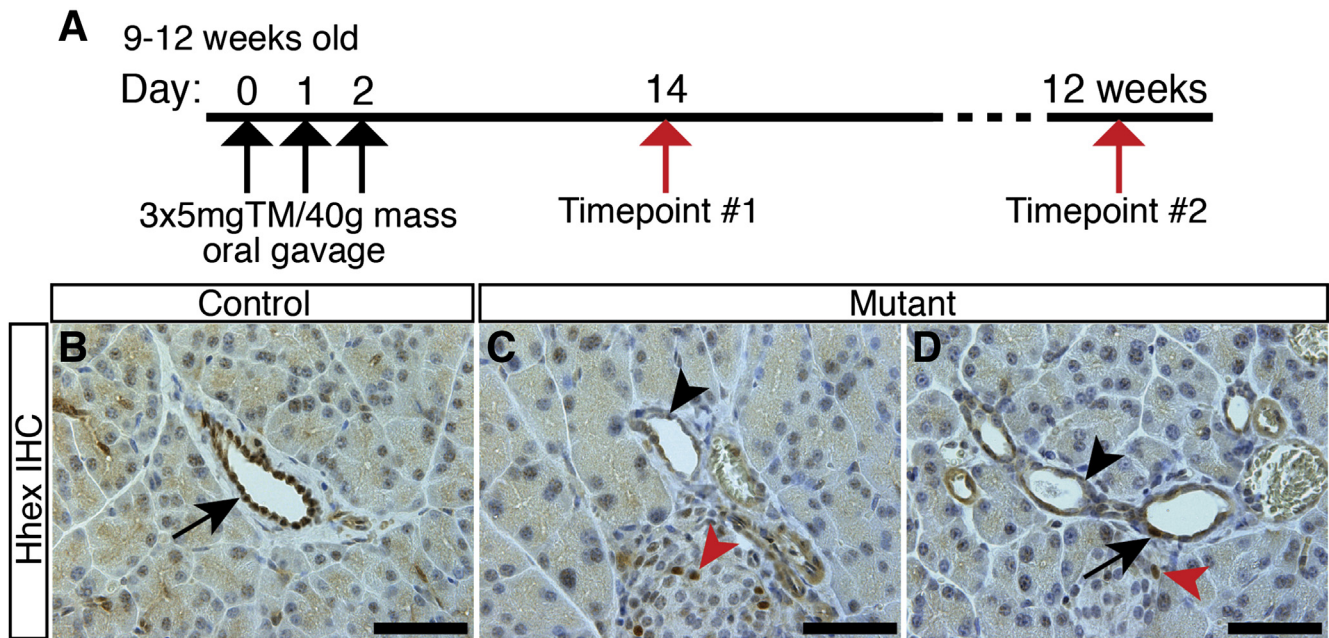For animal studies, dorsal pancreata were dissected in ice-cold PBS and homogenized in TRIzol (15596-026;

Figure 3. Efficient *Hhex* ablation in *Hhex^{loxP/loxP};Sox9-CreER^{T2}* mice. (*A*) Schematic of tamoxifen induction in 9- to 12-week-old mice. (*B–D*) Representative Hhex immunohistochemistry at 2 weeks after induction. (*B*) Littermate controls (*Hhex^{loxP/loxP}*, n = 4) exhibit ducts with nuclear Hhex expression (*black arrow*). (*C, D*) In mutant mice (*Hhex^{loxP/loxP};Sox9-CreER^{T2}*, n = 6), rare escape cells were detected (*black arrow*); 95.7% ± 0.8% of duct cells do not express Hhex (*black arrowheads*) whereas Hhex expression was retained within δ-cells (*red arrowheads*). Scale bars: 50 μm.

Ambion/Life Technologies, Austin, TX). For in vitro studies, cells were washed twice with ice-cold PBS and scraped in 1 mL of PBS. After brief centrifugation at maximum speed, cells were lysed in TRIzol. Total cellular RNA was extracted using the RNeasy Mini Kit (74104; QIAGEN, Valencia, CA). Quantitative reverse-transcriptase PCR was performed as previously described elsewhere.[31] Expression levels were normalized to those of TATA-box binding protein (*Tbp*) as an internal control. Primer sequences for quantitative PCR are provided in Table 3.

For high throughput RNA sequencing, total RNA quantity and quality were assayed with an Agilent 2100 Bioanalyzer (Agilent Technologies, Santa Clara, CA). Libraries were prepared using the TruSeq RNA sample prep kit v2 (Illumina, San Diego, CA). Single-read sequencing was performed on an Illumina hiSeq2000 (100-bp reads) with Casava1.7 software used for base-calling (Illumina). Low-quality reads as well as ribosomal and repeat sequences were filtered out. Remaining reads were aligned to the mouse reference genome (NCBI build 37, mm9) using RNA-Seq unified mapper (RUM) alignment software (University of Pennsylvania School of Medicine, Philadelphia, PA).[32] Differential expression analysis was carried out using EdgeR software (Walter and Eliza Hall Institute of Medical Research, Parkville, Australia).[33]

Pancreatic Ductal Cell Sorting and Culture

Isolation of pancreatic duct cells and culture conditions have been described previously elsewhere.[34] Briefly, pancreata of uninduced 9-week-old *Hhex^{loxP/loxP}* and *Hhex^{loxP/loxP};Sox9-CreER^{T2}* mice were digested in collagenase, and duct cells were isolated via ductal-specific *Dolichos biflorus* agglutinin lectin labeling followed by magnetic bead separation. For recombination experiments, 4-hydroxytamoxifen (H7904; Sigma-Aldrich) was solubilized in ethanol and added to the growth medium at a final concentration of 500 nM.

Cloning of HHEX Overexpression Construct and Lentiviral Transduction

HHEX (Myc-DDK-tagged) ORF (RC204815, Origene Technologies, Rockville, MD; accession number NM_002729) was PCR amplified for subcloning into the pLU.1-IRES-eGFP lentiviral vector using *BamHI* and *AgeI* restriction sites. The primers were BamHI-HHEX-F: 5′-CAC GGATCCGGTACCGAGGAGATC-3′ and AgeI-DDK-R: 5′-GTG ACCGGTTTAAACCTTATCGTCGTCATCCTTG-3′. The thermocycler conditions were as follows: 96°C for 2 minutes, [96°C for 30 seconds, 63°C for 30 seconds, 72°C for 60 seconds] 30 times, 72°C for 10 minutes, and 4°C indefinitely. The final construct was confirmed by sequencing at the NAP-Core Facility at the Children's Hospital of Philadelphia. Lentiviral particles were prepared at the Protein Expression Facility at the Wistar Institute (Philadelphia, PA) and concentrated by ultracentrifugation. Primary ductal cells were transduced by spin transduction at a multiplicity of infection of 1000.[34] Green fluorescent protein positive (GFP+) cells were sorted by fluorescence-activated cell sorting (FACS) 72 hours after transduction at the Flow
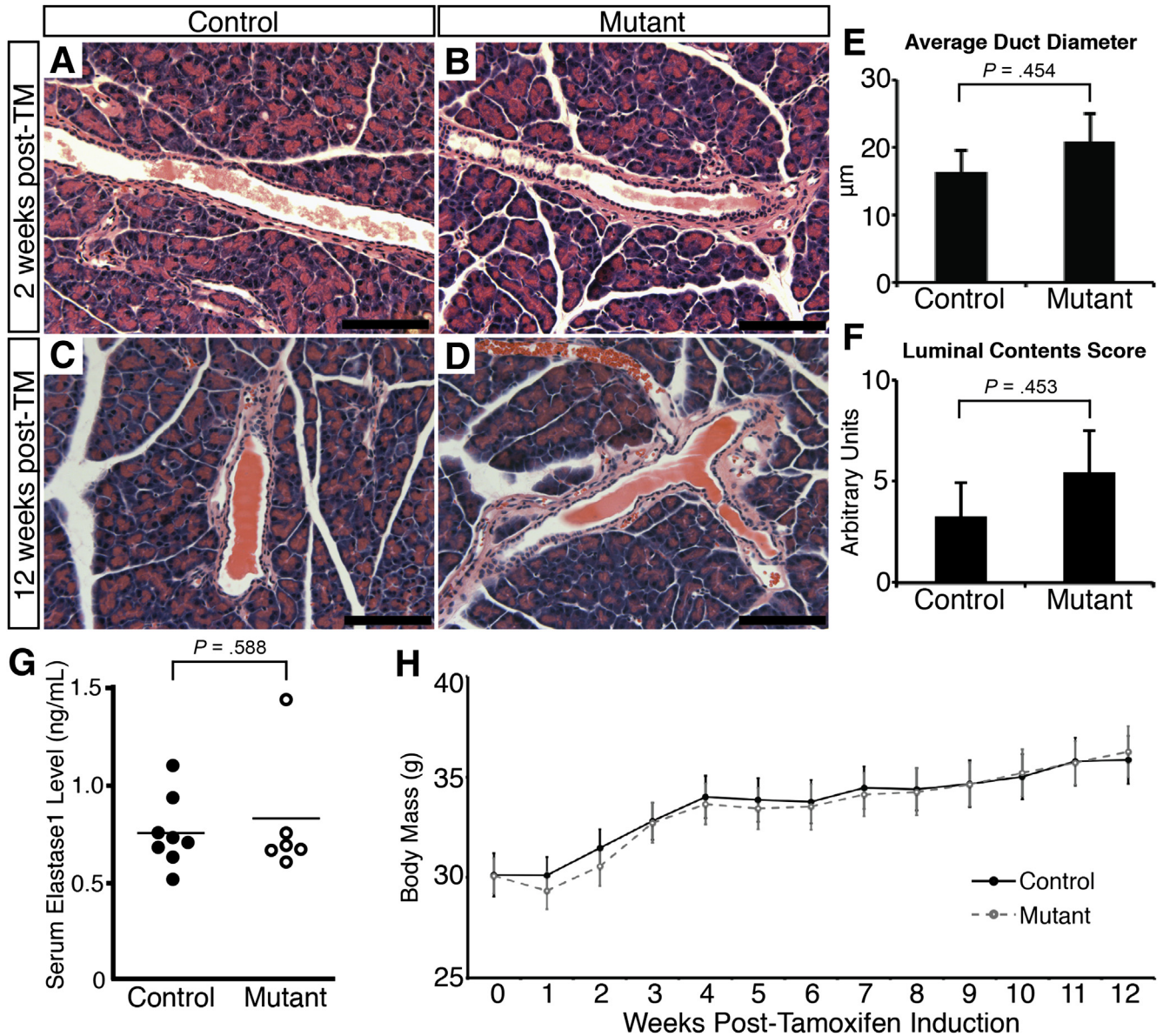
Figure 4. *Hhex* **is not required for maintenance of exocrine compartment homeostasis in the mature pancreas.** (*A–D*) Representative H&E images from littermate control (*Hhex$^{loxP/loxP}$*, n ≥ 4 animals for each time point) and mutant pancreata (*Hhex$^{loxP/loxP}$;Sox9-CreER^{T2}*, n ≥ 6 animals for each time point) display indistinguishable histology at 2 weeks (*A, B*) and 12 weeks (*C, D*) after induction. Scale bars: 100 μm. (*E*) Control (n = 4, mean 16.4 ± 3.1 μm) and mutant (n = 6, mean 20.9 ± 4.1 μm) pancreata exhibit similar ductal diameter 2 weeks after induction (*P* = .454, Student *t* test). Data are presented as the mean of the average diameter of each animal for each genotype ± standard error of the mean. (*F*) Grading of luminal contents (0–10) indicated no statistically significant difference between control (n = 4, mean 3.25 ± 1.70) and mutant (n = 6, mean 5.5 ± 2.01) pancreata 2 weeks after induction (*P* = .453, Student *t* test). (*G*) Similar levels of elastase-1 were detected by enzyme-linked immunosorbent assay in serum of control (n = 8, mean 0.74 ng/mL) and mutant (n = 6, mean 0.83 ng/mL) male mice 10 weeks after induction (*P* = .588, Student *t* test). The mean of each group is indicated. (*H*) Control (n = 8) and mutant (n = 6) male mice were weighed for 12 weeks after induction, with no statistically significant differences in body mass observed at any time point (*P* > .05, Student *t* test).

Cytometry and Cell Sorting Resource Laboratory at the University of Pennsylvania.

Data Access

All RNA-seq data has been deposited to the National Center for Biotechnology Information (NCBI) Gene Expression

Statistical Analysis

At least three animals of each genotype were used for all statistical analyses, as indicated in each experiment. To determine differences between groups, a two-tailed
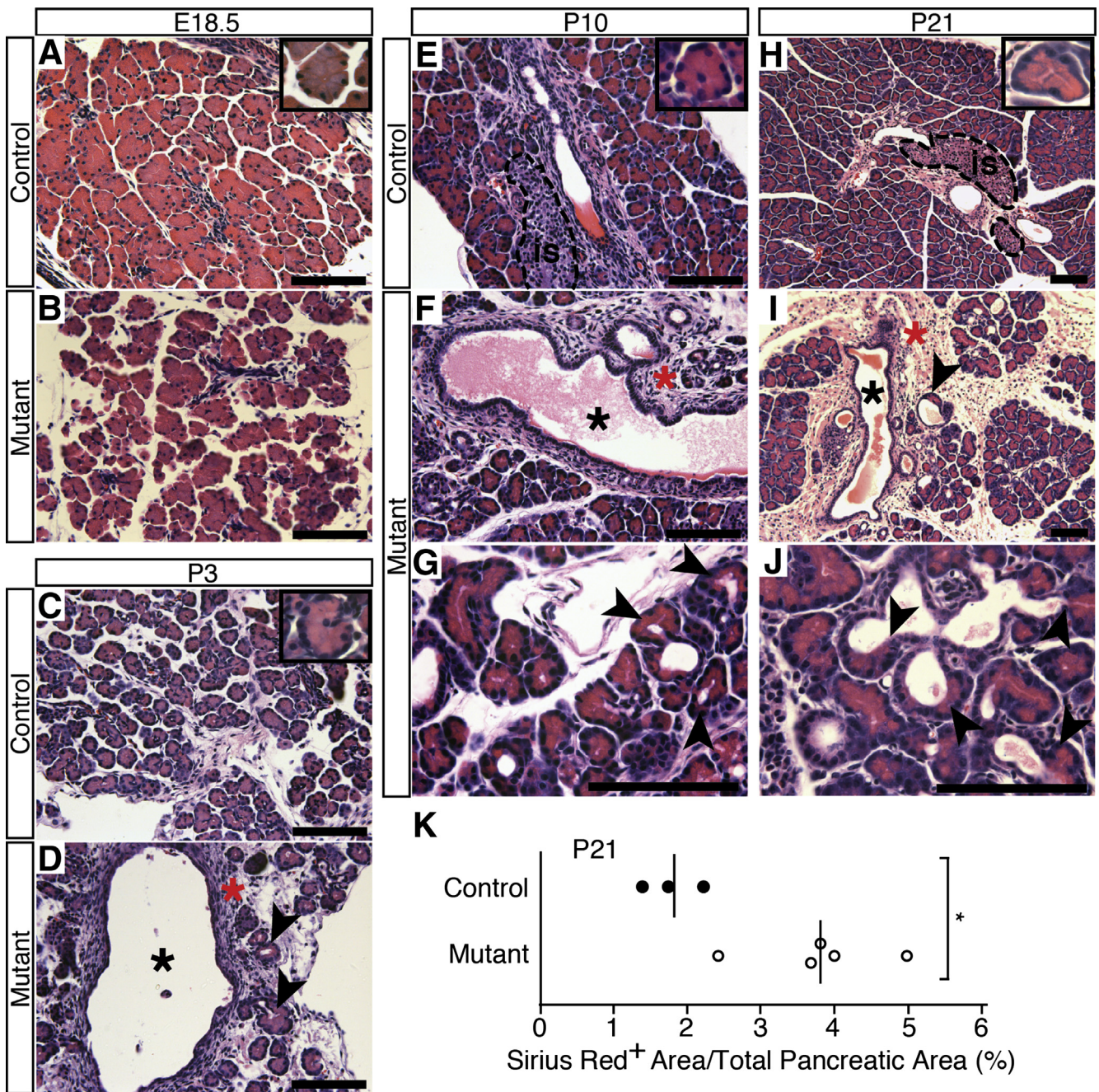
Figure 5. **Perinatal ductal ectasia and acinar-to-ductal metaplasia (ADM) in *Hhex^loxP/loxP;Pdx1-Cre^Early* mice.** (A–J) Representative H&E images at several developmental time points. *Insets*: High-magnification view of an acinus from control pancreas at specific age. (A, B) At embryonic development day 18.5 (E18.5), control (*Hhex^loxP/loxP*, n ≥ 3 animals) and mutant (*Hhex^loxP/loxP;Pdx1-Cre^Early*, n ≥ 3 animals) pancreata displayed similar histology. (C, D) Soon after birth at postnatal day 3 (P3), however, mutants (D, n ≥ 3 animals) showed ectatic ducts (*black asterisk*) with associated periductal fibrosis (*red asterisk*). Moreover, these regions were associated with ADM (*arrowheads*, D, G, I, J), a finding only observed in mutants. (E–G) The histologic features of periductal fibrosis, ductal ectasia, and ADM in mutants became more prominent at P10. (H–J) At P21, severely affected mutant mice exhibited an exacerbated phenotype with concomitant interstitial fibrosis. (K) Fibrotic area was measured by Sirius Red staining in P21 mutant (*Hhex^loxP/loxP;Pdx1-Cre^Early*, n = 5) and control (*Hhex^loxP/loxP*, n = 3) pancreata, and each animal is plotted as a percentage of the total area of the pancreatic footprint. Sirius Red positivity averaged 1.82% in controls and 3.79% in mutants. *$P < .05$. Scale bars: 100 μm; insets: magnification, 400×; *is*, islet.

homoscedastic Student *t* test was performed using Excel software (Microsoft, Redmond, WA). $P < .05$ was considered statistically significant. Variation measurements are given as standard error of the mean. All authors had access to the study data and reviewed and approved the manuscript.
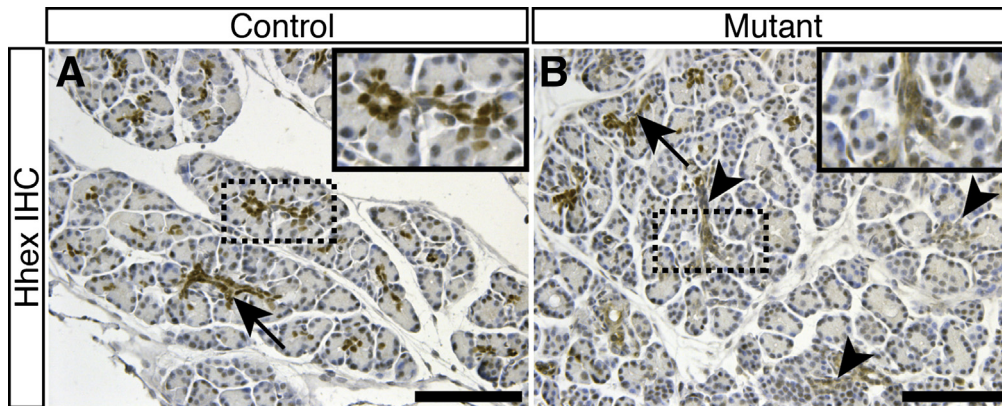
Figure 6. Mosaic *Hhex* expression in *Hhex^loxP/loxP;Pdx1-Cre^Early* mice at P10. (*A*) Representative Hhex immunohisto-chemical staining in control pancreata (*Hhex^loxP/loxP*, n ≥ 3 animals) highlights nuclear Hhex expression in ductal cells (*black arrows*). (*B*) Hhex expression in mutant pancreata (*Hhex^loxP/loxP;Pdx1-Cre^Early*, n ≥ 3 animals) was predominantly a pattern of regional mosaicism in that specific ducts either expressed (*black arrow*) or did not express (*black arrowheads*) Hhex. Similar patterns of mosaicism were observed at postnatal days P3 and P21; 82.8% ± 3.4% of duct cells at P21 (n = 4 mice) lacked Hhex expression. Scale bars: 100 μm. Insets: magnification, 400×.

Results

Hhex *Is Expressed Throughout Developing and Mature Ducts*

To determine the function of *Hhex* in the pancreatic duct, we first characterized its expression dynamics and locali-zation. At E13.5–E18.5, Hhex protein was present in nuclei within $Sox9^+$ cells of the epithelium yet was excluded from $Ngn3^+$ endocrine progenitors during the secondary transi-tion (n ≥ 3 animals for each time point were examined) (Figure 1*A–D* and data not shown). These data indicate that Hhex is expressed in ductal progenitors throughout devel-opment, as the $Sox9^+$ domain becomes progressively more restricted to ductal progenitors during the secondary tran-sition.[30] In postnatal and adult pancreata, Hhex was expressed in all segments of the ductal tree, including cen-troacinar cells, intercalated ducts, intralobular ducts, inter-lobular ducts, and interlobar/main ducts, as well as endocrine δ-cells (see Figure 1*E–G* and data not shown).

Ablation of Hhex *in Pancreatic Progenitors, but Not Mature Ductal Cells, Results in Chronic Pancreatitis*

Because the embryonic lethality of $Hhex^{-/-}$ mice pre-cluded analysis at later stages, we derived two genetic models for conditional *Hhex* ablation to assess the require-ment for *Hhex* in the maintenance of pancreatic duct func-tion at different time points. The pancreata of 18-week-old mice with *Hhex* ablated in pancreatic progenitors (*Hhex^loxP/loxP;Pdx1-Cre^Early*, n = 3) exhibited severe diffuse chronic pancreatitis (40%–85% of footprint affected) with duct ectasia, interstitial and periductal fibrosis, acinar dropout, acinar-to-ductal metaplasia (ADM), and numerous aggre-gates of lymphocytes, plasma cells, and some neutrophils (Figure 2*B* versus *A*). Quantification of these immune cell types confirmed a predominantly lymphocytic infiltrate in

mutants (P = .004 for lymphocytes and P = .03 for neu-trophils; n = 3 for each genotype) (see Figure 2*C*). Ducts were severely ectatic and tortuous, with luminal eosino-philic proteinaceous granular material and cellular debris. The remaining acini were separated into variably sized lobules dissected by variably dense fibrous connective tis-sue (see Figure 2*E*). Consistent with these histologic find-ings of chronic pancreatitis, plasma levels of elastase-1 were elevated 4.2-fold in 8-week-old *Hhex^loxP/loxP;Pdx1-Cre^Early* mice (n = 4) relative to age-matched controls (n = 3; P < .001) (see Figure 2*F*), reflective of acinar cell injury. These data indicate that *Hhex* is required for proper functioning of the exocrine pancreas.

Given the striking pathology of *Hhex^loxP/loxP;Pdx1-Cre^Early* mice, we next tested the hypothesis that *Hhex* is required for maintenance of homeostasis of the exocrine pancreas in the adult. We treated 9- to 12-week-old *Hhex^loxP/loxP;Sox9-CreER^T2* and *Hhex^loxP/loxP* littermate control mice with tamoxifen for 3 consecutive days to induce CreER-mediated deletion of the *Hhex* gene and then analyzed for pancreatic pathology 2 or 12 weeks later (Figure 3*A*). Quantification of Hhex expression in *Hhex^loxP/loxP;Sox9-CreER^T2* mice 2 weeks after induction indicated that 95.7% ± 0.8% (n = 6 mice) of ductal cells had lost Hhex expression as intended, with similar ablation efficiency at 12 weeks after induction (n = 5 mice) (see Figure 3*B–D*). Analysis of H&E stained sections yielded no overt pancreatic pathology at either time point in *Hhex^loxP/loxP;Sox9-CreER^T2* mice compared with littermate controls (Figure 4*A–D*). Moreover, no statistically significant difference in average duct diameter or luminal contents was detected at 2 weeks after induction (see Figure 4*E* and *F*; P = .454 and P = .453, respectively). Finally, measurement of plasma elastase-1 levels by enzyme-linked immunosor-bent assay at 10 weeks after induction showed similar levels between *Hhex^loxP/loxP;Sox9-CreER^T2* (n = 5) and littermate control mice (n = 8; P = .588) (see Figure 4*G*), and no differences in body mass were detectable between these
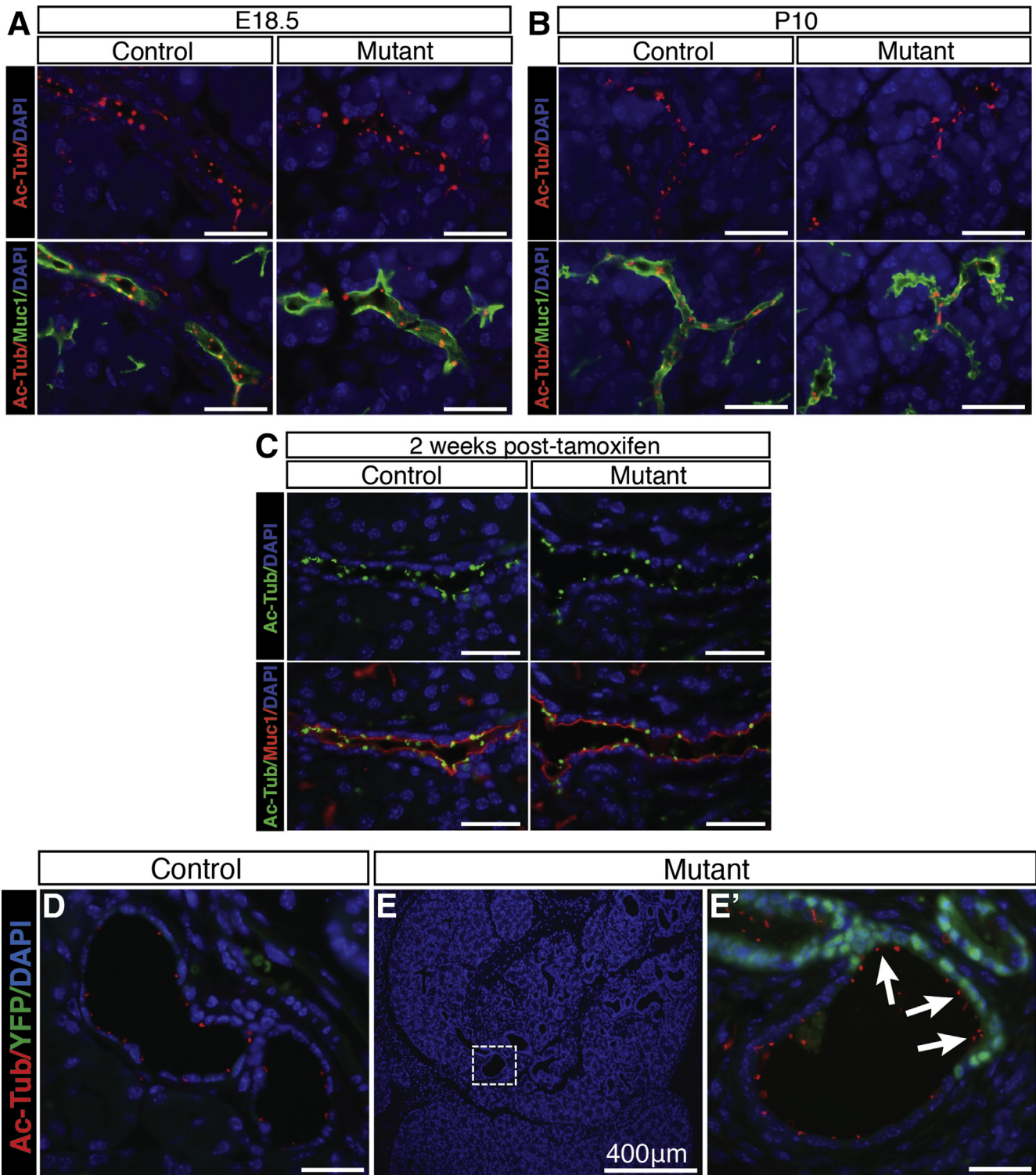
Figure 7. ***Hhex* is not required for expression of primary cilia.** (*A–C*) Immunofluorescence staining for acetylated-tubulin, a marker of primary cilia, in the ductal epithelium. (*A, B*) Acetylated-tubulin (*red*) is visualized within the ductal lumina of both control (*Hhex$^{loxP/loxP}$*) and mutant (*Hhex$^{loxP/loxP}$;Pdx1-Cre^{Early}*) pancreata at embryonic developmental day 18.5 (E18.5) and postnatal day P10 (n ≥ 3 animals for each genotype at each time point). Mucin-1 (*green*) was stained to mark the luminal surface of acinar and ductal cells. (*C*) A similar expression pattern of acetylated-tubulin (*green*) was observed between adult control (*Hhex$^{loxP/loxP}$*) and mutant (*Hhex$^{loxP/loxP}$;Sox9-CreER^{T2}*) pancreata 2 weeks after induction (n ≥ 3 animals for each genotype). Mucin-1 (*red*) highlights ductal lumina. (*D, E'*) Acetylated-tubulin immunofluorescence in P21 control (*Hhex$^{loxP/loxP}$;R26-YFP*, n = 3) and mutant (*Hhex$^{loxP/loxP}$;Pdx1-Cre^{Early};R26-YFP*, n = 4) pancreata indicate the presence of primary cilia intraluminally. Primary cilia were detected on the surface of YFP$^+$ ductal cells (*E', white arrows*) within affected parenchyma, evident on the lower power image of this region (*E*, DAPI only). Scale bars: 25 µm unless noted otherwise.

A

E18.5 Dorsal Pancreas

■ Control
□ Mutant
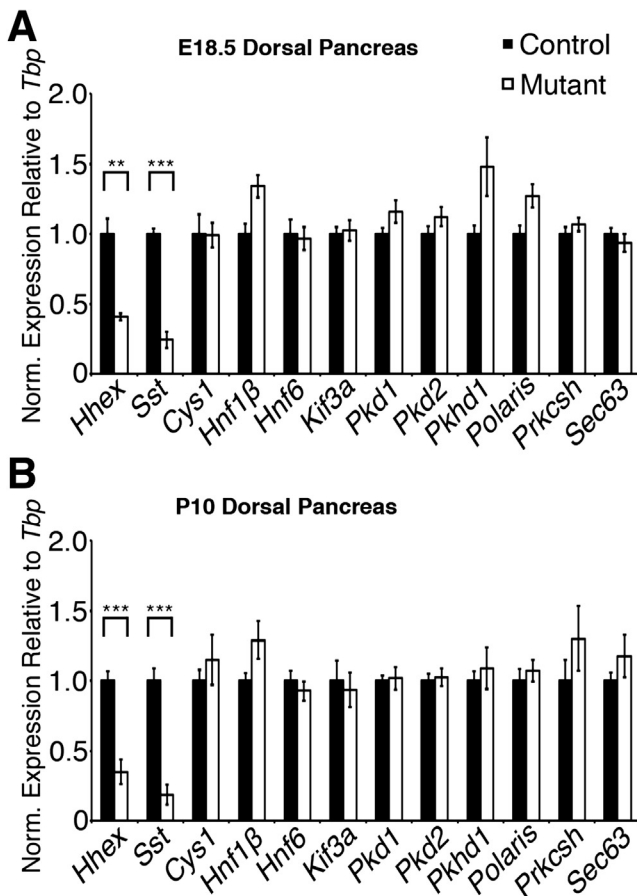

B

P10 Dorsal Pancreas

Figure 8. Expression analysis of genes necessary for primary cilia function. Quantitative reverse-transcription polymerase chain reaction gene expression analysis of dorsal pancreata at embryonic developmental day 18.5 (E18.5) (*A*) and postnatal day P10 (*B*) show similar levels between littermate control mice (*Hhex$^{loxP/loxP}$*, n ≥ 3 animals, *black bars*) and mutant mice (*Hhex$^{loxP/loxP}$;Pdx1-Cre^{Early}*, n ≥ 3 animals, *white bars*) for an array of genes previously implicated in primary cilia formation and function. Somatostatin (*Sst*) was used as a positive control for down-regulation of an established *Hhex* target gene in the pancreas. *Tbp* levels were used to quantify relative gene expression, and the mean of the control group for each gene was normalized to a value of 1. Data are presented as mean ± standard error of the mean. **P < .01, ***P < .001, Student *t* test.

groups for the duration of the study (see Figure 4*H*). Together, these data demonstrate that *Hhex* is not required to maintain homeostasis of the mature pancreatic ductal tree.

Embryonic Loss of Hhex *Leads to Rapid Postnatal Ductal Ectasia Associated With Periductal Fibrosis and Acinar-to-Ductal Metaplasia*

Chronic pancreatitis is a final manifestation of multiple causes of exocrine dysfunction. Therefore, we analyzed *Hhex$^{loxP/loxP}$;Pdx1-Cre^{Early}* mice at earlier time points to determine the most proximal defect, which we reasoned

would uncover the specific function(s) of *Hhex* in ductal epithelial cells. At E18.5, pancreata of *Hhex$^{loxP/loxP}$;Pdx1-Cre^{Early}* mice appeared histologically indistinguishable from those of littermate *Hhex$^{loxP/loxP}$* controls (n ≥ 3 animals for each genotype) (Figure 5*A* and *B*). At P3, however, focal areas of ectatic ducts with periductal fibrosis were evident only in mutants (n ≥ 3 animals for each genotype) (see Figure 5*D* versus *C*). Moreover, these regions were associated with the presence of ADM (see Figure 5*D*, *G*, *I*, and *J*), a finding never observed in control animals. The focal nature of this phenotype is likely resultant of the mosaic pattern of *Hhex* ablation in *Hhex$^{loxP/loxP}$;Pdx1-Cre^{Early}* mice (Figure 6); *Hhex* was observed to be ablated in 82.8% ± 3.4% of duct cells at P21 in mutants (n = 4 animals).

Analysis of pancreata at P10 and P21 (n ≥ 3 animals for each genotype at each time point) indicated that dilation of the exocrine system and extracellular remodeling in mutant mice became progressively more severe (see Figure 5*E–J*). *Hhex$^{loxP/loxP}$;Pdx1-Cre^{Early}* mice (n = 5) at P21 displayed a 2.08-fold increase in fibrotic area measured by Sirius Red stain relative to littermate *Hhex$^{loxP/loxP}$* controls (n = 3; P = .014) (see Figure 5*K*). This progressive pattern of ductal ectasia with concomitant fibrosis in mutants likely accounts for the exocrine dysfunction that leads to chronic pancreatitis in adults.

Hhex *Does Not Cell Autonomously Regulate Expression of Hnf6, Hnf1β, or Primary Cilia in Ductal Cells*

Analysis of *Hhex$^{loxP/loxP}$;Pdx1-Cre^{Early}* pancreata in early life indicated that ductal ectasia was likely a primary cause of subsequent exocrine dysfunction. We therefore reasoned that ectasia was a direct consequence of *Hhex* ablation. Conditional ablation of *Hhex* in embryonic liver has been reported to result in dilated ducts and polycystic liver disease in adulthood.[28] Moreover, expression of the genes encoding the transcription factors Hnf6 and Hnf1β, both of which are known to regulate the elaboration of primary cilia in the pancreas and other organs, was down-regulated in the *Hhex*-ablated liver.[28,35–37] Because pancreas-specific disruption of primary cilia in genetic mouse models results in severe ductal ectasia and subsequent chronic pancreatitis, we hypothesized that Hhex may regulate a transcription factor cascade that includes Hnf6, Hnf1β, and the genes necessary for functioning of primary cilia.[38,39]

Typically, primary cilia are present exclusively on ductal and islet cells in the pancreas from midgestation onward. Therefore, we determined the presence of primary cilia both before (E18.5) (n = 3 for each genotype) and after (P10) (n = 3 for each genotype) the emergence of ductal ectasia (Figure 7*A* and *B*). At both time points, primary cilia were clearly evident on the luminal surface of ductal cells in our *Hhex* ablation model.

Additionally, we assayed for the presence of primary cilia in the adult model of *Hhex* ablation and observed similar numbers of primary cilia between *Hhex$^{loxP/loxP}$;Sox9-CreER^{T2}* and *Hhex$^{loxP/loxP}$* littermate control mice (n = 3 for each genotype) (see Figure 7*C*). To ensure that expression of
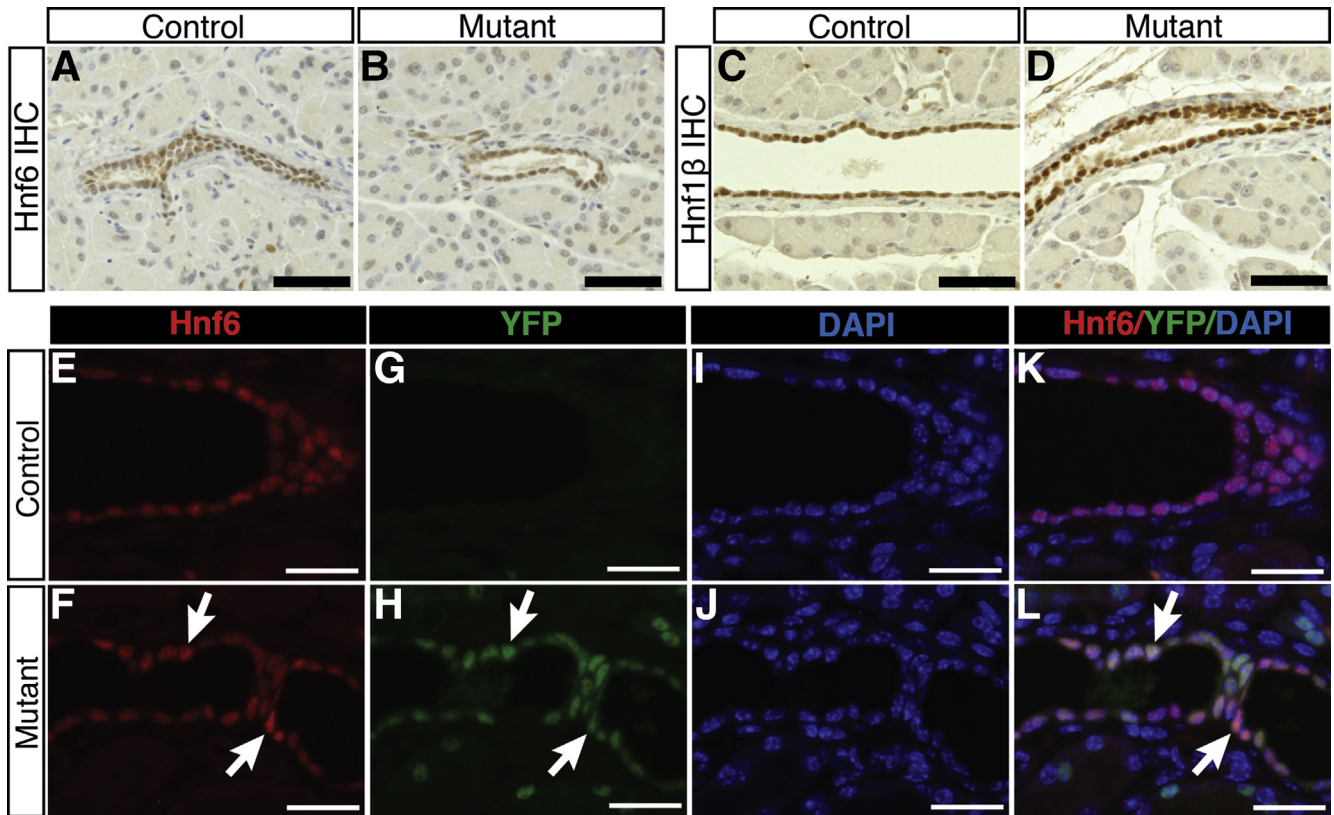
Figure 9. *Hhex* **is not required for expression of Hnf6 or Hnf1β.** (*A*) Representative immunohistochemical analysis for Hnf6 (*A, B*) and Hnf1β (*C, D*) indicates similar levels of protein between controls (*Hhex*$^{loxP/loxP}$, n = 3 animals) and mutants (*Hhex*$^{loxP/loxP}$; *Sox9-CreER*^{T2}, n = 3 animals) 2 weeks after induction in the ductal epithelium. Scale bars: 50 μm. (*E–L*) Similar levels of Hnf6 were expressed in ductal cells of control (*Hhex*$^{loxP/loxP}$;*R26-YFP*, n = 3) and mutant (*Hhex*$^{loxP/loxP}$;*Pdx1-Cre*^{Early};*R26-YFP*, n = 3) pancreata at postnatal day P21. Hnf6 was detected in YFP$^+$ cells (*F, H, L, white arrows*). Scale bars: 25 μm.

primary cilia is indeed not cell-autonomously regulated by *Hhex*, we derived an additional mouse model, *Hhex*$^{loxP/loxP}$; *Pdx1-Cre*^{Early};*R26-YFP*, in which *Cre* recombinase activity indelibly marks a pancreatic progenitor cell and its progeny with yellow fluorescent protein (YFP) expression. Primary cilia were clearly expressed by YFP$^+$ cells in *Hhex*$^{loxP/loxP}$;*Pdx1-Cre*^{Early};*R26-YFP* mutants (n = 4) at P21, including in areas of ductal ectasia (see Figure 7*E* and *E′*).

Although primary cilia were present on ductal cells of mutant pancreata in both genetic models of *Hhex* ablation, the possibility remained that the functioning of these organelles was compromised. To address this possibility, we performed gene expression analysis at E18.5 and P10 for an array of genes that have previously been implicated in primary cilia formation and/or function in both the pancreas and other organs.[35,37] At both ages, no significant decrease in the mRNA levels of any of these genes was detected (Figure 8).

Notably, transcript levels of *Hnf6* and *Hnf1β* were similar between mutants and littermate controls at both E18.5 and P10 (see Figure 8), in contrast to what has been reported for protein expression in embryonic liver-specific *Hhex* ablation.[28] It is important to note that these two factors are nearly duct-specific in the P10 pancreas, excluding the possibility that residual expression in other cell types accounted for the lack of alteration in gene

expression.[30,40–42] To confirm that these factors are indeed not cell-autonomous targets of Hhex in the pancreas, we analyzed their expression pattern in induced adult *Hhex*$^{loxP/loxP}$;*Sox9-CreER*^{T2} pancreata (n = 5). Similar levels of each protein were detected in mutants and controls 2 weeks after induction (Figure 9*A–D*). The expression pattern of Hnf6 in *Hhex*$^{loxP/loxP}$;*Pdx1-Cre*^{Early};*R26-YFP* mutant pancreata (n = 3) appeared similar to that of littermate controls (n = 3) at P21 (see Figure 9*E* and *F*). Notably, Hnf6 was clearly detectable in YFP$^+$ cells (see Figure 9*L*). Together, these data show that *Hhex* ablation in the pancreas does not affect expression of *Hnf6*, *Hnf1β*, or primary cilia genes in a cell-autonomous manner, which points toward a different function of Hhex in the pancreas compared to the liver.

Hhex Ablation Results in Changes Consistent With Ductal Hypertension

Given the coincident onset of ductal ectasia with postnatal exocrine activation in *Hhex*$^{loxP/loxP}$;*Pdx1-Cre*^{Early} mice, and the fact *Hhex* regulates functional genes in a variety of mature cell types, we next hypothesized that *Hhex* directly contributes to the regulation of ductal cell function—that is, secretion. Importantly, the progressive manner of the pathologic changes of *Hhex*$^{loxP/loxP}$;*Pdx1-Cre*^{Early} mice closely resembles   that   of   the   primary   pancreatic   ductal
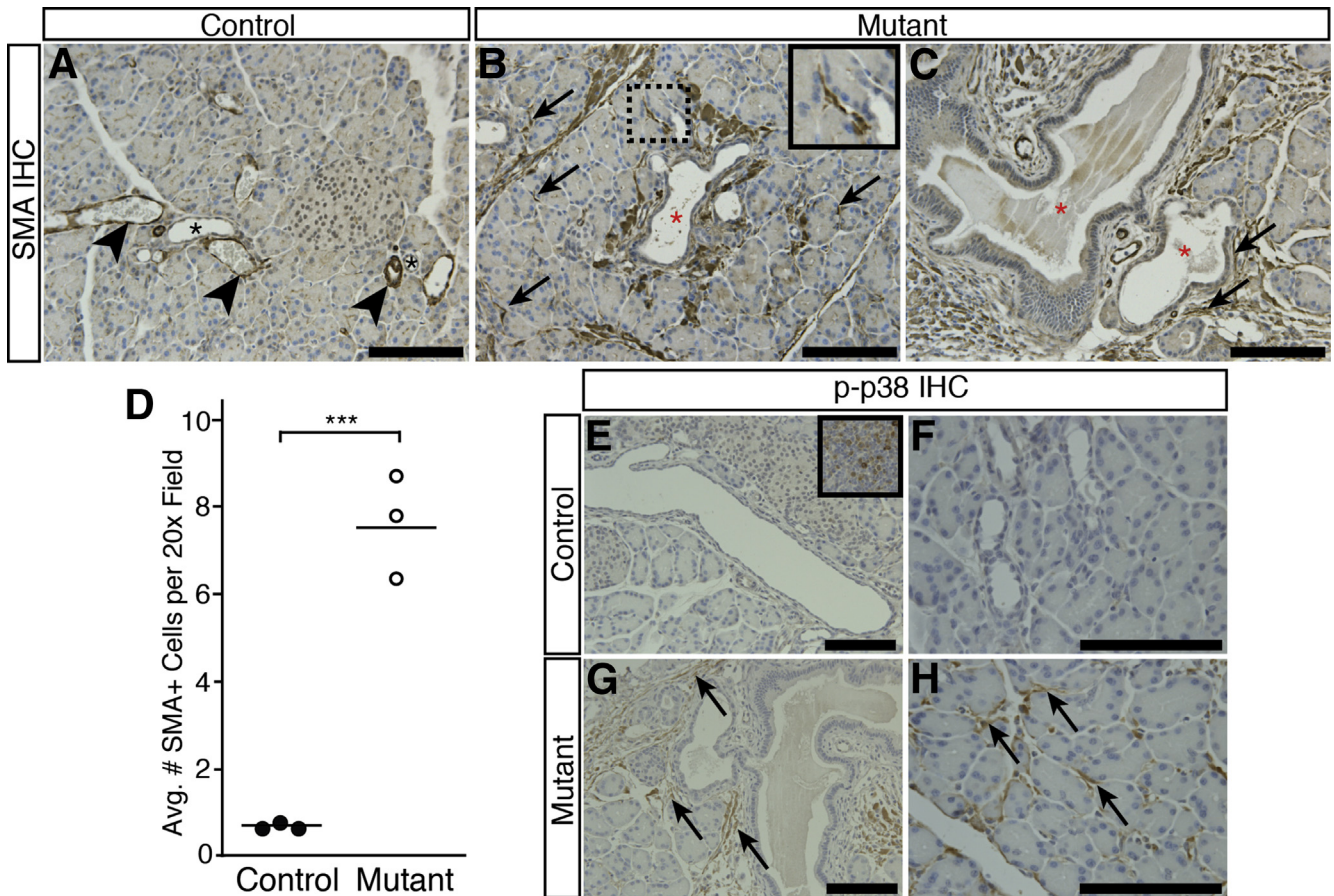
Figure 10. Activated pancreatic stellate cells (PSCs) are present in pancreata of *Hhex*^loxP/loxP^;*Pdx1-Cre*^Early^ mice. (A–C) Immunostaining for smooth muscle actin (SMA) was used as a marker for activated PSCs. (A) In postnatal day P21 control mice (*Hhex*^loxP/loxP^, n = 3), SMA expression was evident exclusively in the vasculature of the pancreas (*arrowheads*). *Black asterisks*: ducts. (B, C) P21 mutant pancreata (*Hhex*^loxP/loxP^;*Pdx1-Cre*^Early^, n = 3), however, exhibited significant smooth muscle actin (SMA) expression (*black arrows*) within the parenchyma surrounding ectatic ducts (*red asterisks*) and histologically normal acini. *Inset*: Fibroblastic-type SMA$^+$ cell abutting an acinus. (D) The number of SMA$^+$ cells was quantified in 20 random magnification 20× fields of mutant (*Hhex*^loxP/loxP^;*Pdx1-Cre*^Early^, n = 3) and control (*Hhex*^loxP/loxP^, n = 3) pancreata, and the average number of SMA$^+$ cells per magnification 20× field is plotted for each animal. Mutant pancreata demonstrated a significantly increased average number of SMA$^+$ cells (mutant genotype average 7.55) relative to littermate controls (control genotype average 0.65). ***$P < .001$, Student t test; bars indicate mean of genotype. (E–H) Immunostaining for phosphorylated p38 (p-p38) stress kinase in P21 pancreata. (E, F) p-p38 parenchymal reactivity was not observed within control tissue (n = 2). *Inset*: Immune cells within an intrapancreatic lymph node were used as an internal positive control. (G, H) p-p38 immunore-activity within mutant pancreata (n = 2) demonstrated a similar pattern as that for SMA in that p-p38$^+$ fibroblastic-type cells (*black arrows*) were observed surrounding ectatic ducts and adjacent acini. Scale bars: 100 μm.

hypertension model.[26] In this model, the pancreatic duct of rats is cannulated and attached to a pump to cause primary ductal hypertension by physical means, and the common bile duct is diverted directly to the duodenum to avoid hepatic hypertension. The first-observed pathologic changes in the pancreas in this model were ectatic ducts with peri-ductal fibrosis, which ultimately proceeded to interstitial fibrosis and chronic pancreatitis, an overall pathogenesis similar to that seen in *Hhex*-deficient mice (see Figure 5). Therefore, we hypothesized that *Hhex* ablation in the ductal epithelium results in hypersecretion and its sequelae.

To test this hypothesis directly, we attempted to cannulate the ampulla of Vater for direct volumetric assessment of pancreatic secretions; unfortunately, these attempts were unsuccessful due to the extremely small diameter of the ampulla in mice. As a surrogate for barostress, we therefore assayed for the presence of activated pancreatic stellate cells (PSCs). One of several mechanisms by which PSCs are activated is direct pressure, leading to a signaling cascade via phosphorylation of the stress kinase p38.[26,43] Consistent with this finding, widespread activation of PSCs had been observed in the ductal hypertension model by staining for SMA.[26,43] Concordantly, pancreata of P21 *Hhex*^loxP/loxP^;*Pdx1-Cre*^Early^ mice (n = 3) exhibited SMA$^+$ cells most prominently within fibrotic areas of ectatic ducts (Figure 10B and C), abutting histologically normal-appearing acini adjacent to affected regions (see Figure 10B), and within areas of interlobar fibrosis (data not shown). In contrast, control
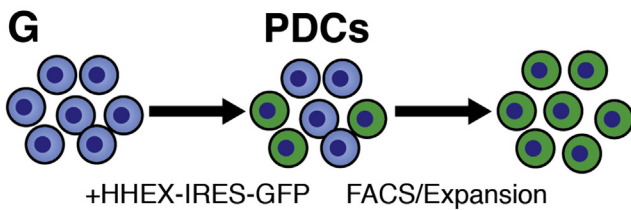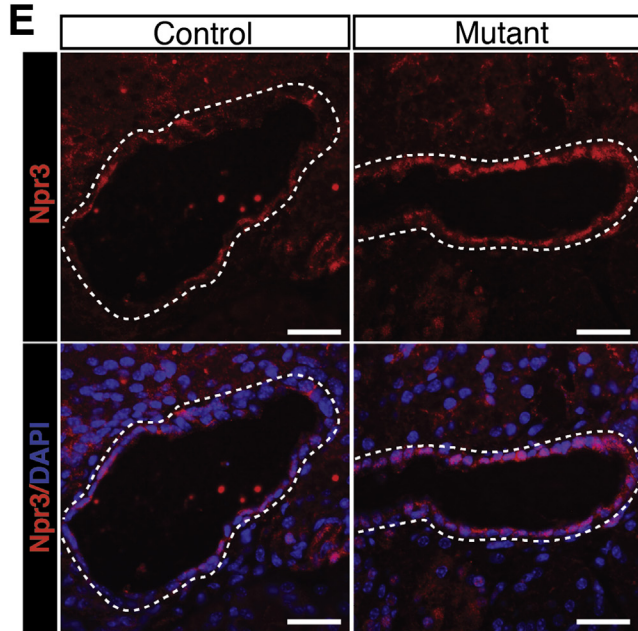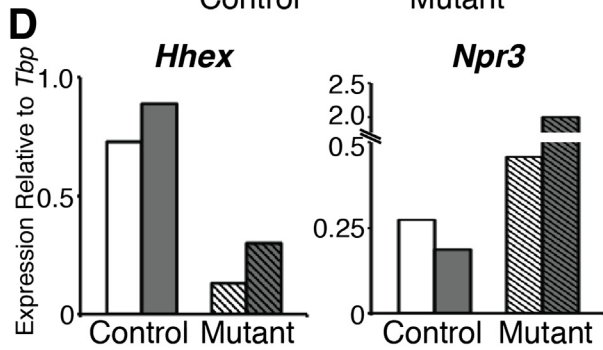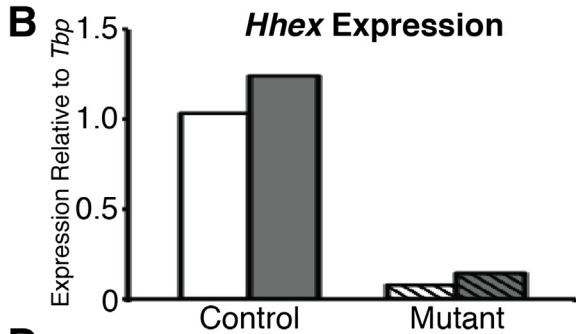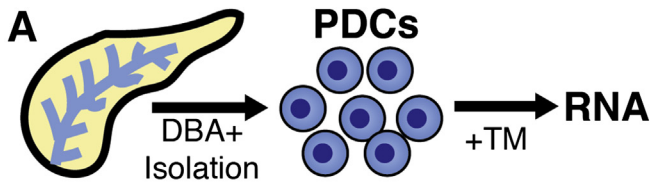
C

Gene Symbol	Fold Change	p-value	Avg. RPKM Controls
Receptors			
Vmn2r29	9.66	0.000435	0.0581
Npr3	4.70	8.17E-06	2.86
Cnr1	2.66	0.000551	0.384
Transporters/Channels			
Aqp5	14.3	0.000941	0.964
Scnn1g	7.57	1.00E-09	0.226
Slc25a48	3.64	3.25E-05	3.19
Slc16a12	3.05	8.85E-05	0.412
Scnn1a	2.37	1.46E-06	3.12
Slc43a3	2.19	0.000163	2.47
Abcb1b	2.16	3.28E-06	35.5
Abcc5	1.82	0.000450	15.3
Cacna1h	-4.39	0.000214	0.481
Slc16a3	-4.22	4.41E-07	5.42
Slc28a3	-4.08	6.50E-06	2.08
Slc22a4	-2.92	1.26E-06	15.6
Signal Transduction Regulators			
Wnk1	1.76	0.000625	11.3
Rgs2	-2.08	7.00E-05	8.03
Rgs16	-2.07	0.000113	65.6
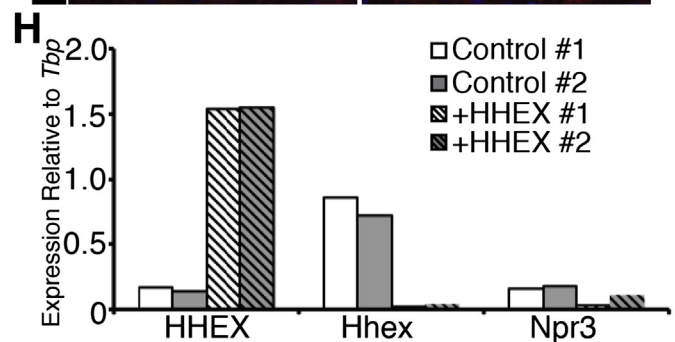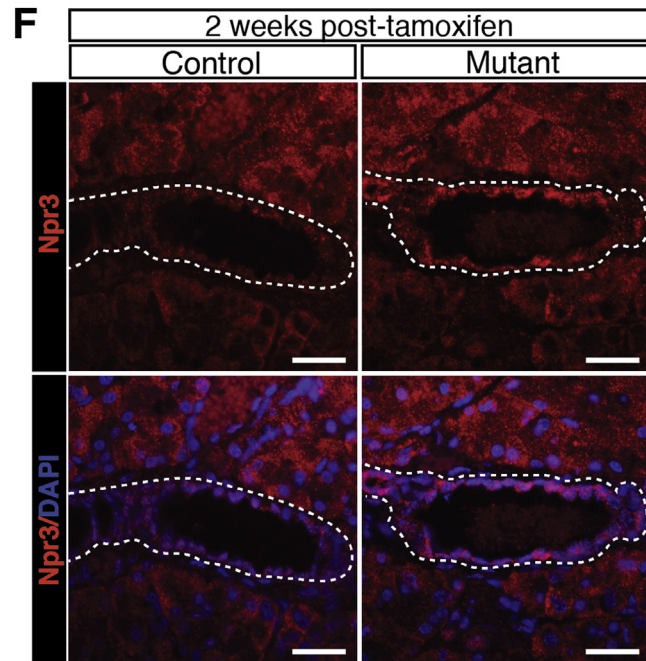
pancreata (n = 3) showed SMA immunoreactivity only in the vasculature (see Figure 10*A*). Quantification of the average SMA$^+$ cell number per field indicated a 11.6-fold increase in mutants (n = 3 for each genotype, $P < .001$) (see Figure 10*D*). Moreover, immunostaining for phosphorylated p38 (p-p38) in P21 tissue showed a similar pattern as that for SMA, in that only mutant pancreata had p-p38$^+$ fibroblastic-type cells within areas of periductal fibrosis and surrounding acini (see Figure 10*E–H*). These data are consistent with widespread activation of PSCs as a consequence of ductal hypertension, although other mechanisms cannot be excluded.

Hhex *Cell-Autonomously Represses* Npr3 *in Ductal Cells*

To determine the molecular basis of ductal ectasia, we performed transcriptome analysis using *Hhex*-ablated primary ductal cells (PDCs). Due to the numerous secondary effects evident in *Hhex*$^{loxP/loxP}$;*Pdx1-Cre*^{Early} mice, such as inflammatory infiltrates, PSC activation, and remodeling of extracellular matrix, we elected to use an ex vivo system to ablate *Hhex* acutely in PDCs to ascertain the most proximal gene expression changes. PDCs were isolated from uninduced control *Hhex*$^{loxP/loxP}$ and mutant *Hhex*$^{loxP/loxP}$;*Sox9-CreER*^{T2} mice to establish PDC lines (Figure 11*A*; n = 2 for each genotype). Upon 4-hydroxytamoxifen administration in vitro, both *Hhex*$^{loxP/loxP}$;*Sox9-CreER*^{T2} mutant lines showed dramatically reduced levels of *Hhex* transcript relative to control lines, as expected (see Figure 11*B*). High-throughput sequencing of RNA-derived libraries yielded a total of 216 differentially expressed transcripts (152 upregulated, 64 down-regulated; FDR <0.10) in *Hhex*-ablated PDCs versus controls. Of these, we focused on genes that could be implicated in ductal secretion (ie, G-protein coupled receptors, ion transporters/channels, and regulators of G-protein coupled receptor downstream signaling) (see Figure 11*C*).
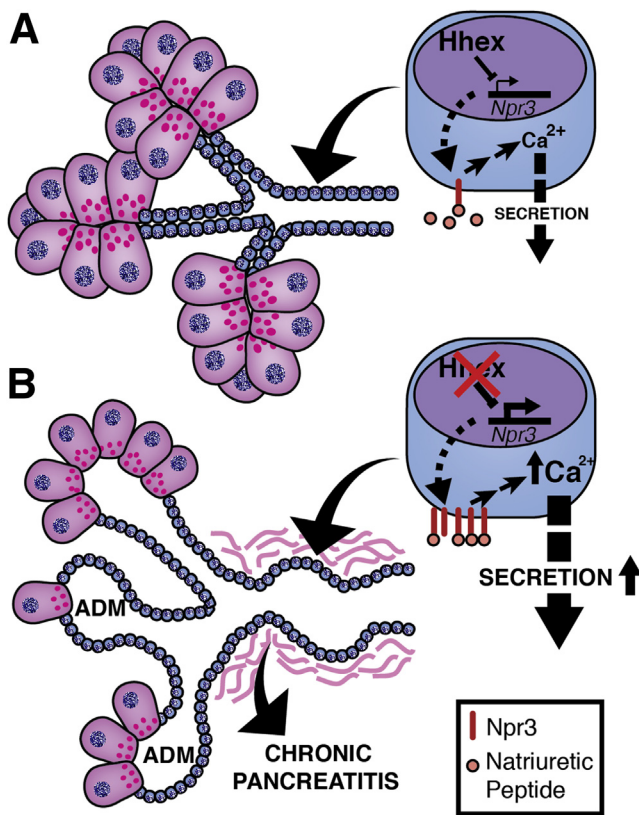
We selected the gene natriuretic peptide receptor 3 (*Npr3*) for follow-up analysis because it showed a 4.70-fold increase in *Hhex*-ablated PDCs, is expressed at a higher level than other differentially regulated G-protein coupled receptors in PDCs (see Figure 11*C*) and has previously been shown to potentiate secretin signaling to enhance pancreatic flow in vivo.[27] Increased levels of *Npr3* transcript were detected in an independent experiment, validating results from the transcriptome analysis (see Figure 11*D*). Immunostaining for Npr3 in both genetic models confirmed increased Npr3 protein levels specifically in the *Hhex*-ablated ductal epithelium while Npr3 levels within the acinar cells remained unchanged (see Figure 11*E* and *F*). To support the hypothesis that Hhex functions to repress the *Npr3* locus, we performed the converse experiment to our aforementioned approach, reasoning that Hhex overexpression should reduce *Npr3* levels. Thus, PDCs were transduced with a HHEX-IRES-GFP lentiviral construct and sorted by FACS to establish HHEX-overexpressing PDC lines (see Figure 11*G*). Gene expression analysis indeed showed a reduction of *Npr3* levels relative to control lines (0.104 and 0.029 for HHEX overexpressers, versus 0.173 and 0.155 for controls) (see Figure 11*H*). Intriguingly, overexpression lines showed a concomitant, dramatic reduction of murine *Hhex* transcript (0.0349 and 0.0212 versus 0.722 and 0.859), suggesting that Hhex may participate in an autoregulatory feedback loop in pancreatic ductal epithelial cells.

Discussion

The results presented above support a model in which the homeobox transcription factor *Hhex* serves an essential role in maintenance of exocrine homeostasis in early life by dampening the response of ductal cells to stimulatory signals, thus preventing hypersecretion (see model in Figure 12). According to our model, *Hhex* ablation in pancreatic progenitors results in increased expression of the G-protein coupled receptor *Npr3* specifically in ductal cells; this raises the effective concentration of paracrine natriuretic peptide signals, which produces a primary hypersecretion defect of the ductal epithelium. The resultant ductal hypertension leads not only to ductal ectasia but also to activation of pancreatic stellate cells, which can mediate the processes of periductal fibrosis, inflammation, and immune

Figure 11. (*See previous page*). ***Hhex* regulates *Npr3* expression cell-autonomously in pancreatic ductal cells.** (*A*) Schematic of approach to identify cell autonomous targets of *Hhex*. *Dolichos biflorus* agglutinin positive ductal cells were isolated from pancreata of 9-week-old control mice (*Hhex*$^{loxP/loxP}$, two animals) or mutant mice (*Hhex*$^{loxP/loxP}$;*Sox9-CreER*^{T2}, two animals) to establish primary ductal cell (PDC) lines. Treatment with 4-hydroxytamoxifen was used to induce recombination in vitro. (*B*) Gene expression analysis for *Hhex* transcript levels 4 days after 4-hydroxytamoxifen treatment. (*C*) Partial list of the 216 transcripts identified to be differentially regulated in *Hhex*-ablated PDCs by RNA-seq (false discovery rate <0.10). Genes were selected based on their potential to regulate ductal secretion via receptor signaling, ion transport, or signal transduction capability. The fold change is presented as mutant/control. The reads per kilobase per million mapped reads values of the two control lines were averaged to give an indication of relative expression level. (*D*) An independent experiment was performed to validate gene expression changes identified by transcriptome analysis. RNA was collected 48 hours after 4-hydroxytamoxifen treatment. *Hhex* and *Npr3* expression levels are both presented relative to *Tbp*. (*E, F*) Immunofluorescence staining for Npr3 shows higher levels specifically within the ductal epithelium of mutants. (*E*) Postnatal day P21 mutant mice (*Hhex*$^{loxP/loxP}$;*Pdx1-Cre*^{Early}, two animals) versus control mice (*Hhex*$^{loxP/loxP}$, two animals). DAPI was used to visualize nuclei. Ductal epithelium is outlined. Scale bars: 25 μm. (*F*) Adult mutant mice (*Hhex*$^{loxP/loxP}$;*Sox9-CreER*^{T2}, n = 2) versus control mice (*Hhex*$^{loxP/loxP}$, n = 2) 2 weeks after induction with tamoxifen. DAPI was used to visualize nuclei. Ductal epithelium is outlined. Scale bars: 25 μm. (*G*) Schematic of *HHEX* overexpression approach. Two primary ductal cell lines were transduced with a lentivirus containing a HHEX-IRES-GFP construct. GFP$^+$ cells were sorted by fluorescence-activated cell sorting 72 hours after transduction to establish *HHEX*-overexpressing PDC lines. (*H*) Gene expression analysis of control (n = 2) and *HHEX*-overexpressing (n = 2) PDC lines for *HHEX*, *Hhex*, and *Npr3* is presented relative to *Tbp*.

Figure 12. Model of *Hhex* molecular function in the pancreatic ductal epithelium. (*A*) In control pancreata, *Hhex* functions to repress expression from the *Npr3* locus. Signaling pathways in the ductal cell contribute to physiologically appropriate secretion that maintains homeostasis of the exocrine pancreas. (*B*) When *Hhex* is ablated in pancreatic progenitors, however, Npr3 protein levels are increased specifically in ductal cells. Upon postnatal activation of the exocrine pancreas, the effective concentration of natriuretic peptide ligand at the ductal cell surface is raised, resulting in hypersecretion. Consistent with primary ductal hypertension, ectatic ducts with periductal fibrosis are evident, and disruption of exocrine homeostasis results in acinar-to-ductal metaplasia. Ultimately, destruction and remodeling of parenchyma will manifest as chronic pancreatitis.

cell recruitment.[44,45] The interstitial pressure within pancreata from human patients with chronic pancreatitis has been reported to be over 10-fold higher than normal;[46] thus, we contend that the fibrotic process exhibited in perinatal life initiates a cascade of events that serve as a positive feedback loop, further increasing intraductal pressure and extracellular remodeling, ultimately manifesting as chronic pancreatitis later in life.

Natriuretic peptide signaling is best characterized for its role in cardiovascular homeostasis;[47,48] however, most of the gastrointestinal tract has been described as a site of production of atrial natriuretic peptide (ANP).[49,50] Fluctuations of ANP expression in the gastrointestinal tract in fed versus fasted states support its role as a paracrine signaling mediator.[51] In the pancreas, ANP is most highly expressed in acinar and centroacinar cells.[52,53] Intravenous

administration of ANP in rats results in decreased chloride and increased bicarbonate concentrations in pancreatic juice.[27] Consistent with these molecular studies, ANP signaling, mediated via the phosphatidylinositol pathway downstream of Npr3, synergizes with secretin signaling to increase pancreatic flow rate, a physiologic metric that is contingent upon active transport of bicarbonate across the ductal epithelium.[27] Our transcriptome analysis of primary ductal cells is the first to indicate that *Npr3* is the most highly expressed natriuretic peptide receptor in this cell type, thus likely accounting for the aforementioned physiologic functions (average normalized expression [reads per kilobase per million mapped reads] values of control PDCs: *Npr1* 0.16; *Npr2* 0.94; *Npr3* 2.86).

Identifying paracrine signaling molecules released from acinar cells and determining their relevance to pancreatic function and pathology is an ongoing effort. Proteomic analysis of pancreatic acinar zymogen granules identified 371 proteins, many of which are secreted and/or have unknown function.[54] In addition to peptides, an extensive list of other signaling molecules has been described; among these are Ca^{2+} and adenosine-5'-triphosphate (ATP), capable of mediating signals on ductal cells via luminal calcium-sensing G-protein coupled and iono-/metabotropic purinergic receptors, respectively.[55,56] Moreover, Behrendorff et al[57] reported that exaggerated intraluminal acidification caused by proton release from secretory granules of acinar cells in response to supraphysiologic activation directly contributes to pancreatitis via perturbation of tight junctions. Although the function of intraluminal acinar acidification is not entirely clear at this time, it may serve as a negative feedback mechanism to prevent acinar hypersecretion by inhibiting acinar cell endocytosis;[58] thus, this report highlights a direct link between paracrine mediators and disease pathogenesis. To the best of our knowledge, our study is the first to describe a pathogenic mechanism in the exocrine pancreas implicating a paracrine signaling pathway as the primary defect.

It is important to note that our study does not exclude formally the possibility of either a primary morphologic defect of the ductal tree or a functional requirement for *Hhex* outside the ductal lineage not detected by simple histology at E18.5. We believe these possibilities to be less likely for several reasons. First, genetic ablation of loci encoding transcription factors, such as *Sox9* or *Hnf6*, that result in morphological phenotypes often manifest in early or mid-pancreatic development.[35,59] Second, our data indicate that ductal ectasia in *Hhex*-deficient mice occurs only after birth, and thus is coincident with exocrine activation upon feeding. Hezel et al[60] described a similar scenario in which conditional pancreatic ablation of *Lkb1* resulted in apparently normal pancreata at birth; however, mice rapidly developed pancreatic inflammation and acinar degeneration only after birth due to defective acinar cell polarity and tight junctions. Likewise, in our study, a phenotype contingent upon paracrine signaling would manifest only after activation of the exocrine system postnatally. Finally, the overall progression of pancreatic pathology we observed is consistent with the primary ductal hypertension model.[26]

Together, these data establish a role for *Hhex* and highlight the importance of paracrine signaling in maintaining normal pancreatic duct secretion, particularly in neonates.

Although *Hhex* is crucial for maintenance of exocrine homeostasis in early life, it is dispensable in the mature duct. It remains unclear, however, why elevated Npr3 levels in the ductal epithelium of adult *Hhex*^{loxP/loxP};*Sox9-CreER*^{T2} mice do not result in ductal ectasia or fibrosis. We propose at least four possibilities to account for the discrepancy between our genetic models. 1) Newborn animals are fed a diet consisting exclusively of milk, which has a much higher fat content than normal rodent chow. Cholecystokinin levels—and thus acinar paracrine signals—would presumably be increased on a high-fat diet, thereby exacerbating *Npr3*-mediated ductal hypersecretion. 2) The smaller average caliber of the perinatal ductal tree relative to that of the adult mouse may predispose younger mice to the sequelae of hypersecretion. Resistance to flow, and thus pressure, is inversely related to the fourth power of the radius of a tube; therefore, minor increases in the volume of secretion in early life may lead to a more drastic increase in pressure compared to adulthood, and this increase may pass a critical threshold for activation of pancreatic stellate cells. 3) The extracellular matrix of perinatal ducts may not be able to safeguard against increased pressure compared to a mature duct, and/or the adult duct is more responsive to adapt to pressure fluctuations by altering extracellular matrix through posttranslational modification (such as collagen crosslinking). More compliant ducts in perinatal mice would become ectatic in response to intraductal hypertension caused by *Hhex* ablation, and this force would be more readily transmitted to the interstitial space, thus resulting in PSC activation. 4) The mature exocrine pancreas, including both acinar and ductal cells, may contain a negative feedback control mechanism lacking in the immature pancreas that is responsive to the volume of secretions. Of course, these possibilities are not mutually exclusive, and some or all may contribute to the propagation of ductal ectasia and fibrosis in early life only.

Given the early onset and progressive nature of the phenotype in *Hhex*-ablated pancreata, it is tempting to speculate whether mutations in *HHEX*, or possibly other loci that result in ductal hypersecretion, are plausible etiologies of hereditary or idiopathic chronic pancreatitis in humans. Often, hereditary chronic pancreatitis (HCP) presents in childhood or adolescence, and a majority of patients with hereditary pancreatitis possess a mutation (or rarely an amplification) in the cationic trypsinogen gene (*PRSS1*).[61–63] Gain-of-function mutations in *PRSS1* lower the threshold for autoactivation of trypsinogen into active trypsin within the pancreas, thus resulting in pancreatitis.[64] Mutations of *PRSS1*, however, are found only in 52% to 68% of patients with HCP, leaving a large contingent of patients with unexplained etiology.[61–63]

Since the discovery of *PRSS1* mutations as a cause of HCP, other loci have been implicated as genetic modifiers of both HCP and idiopathic chronic pancreatitis (ICP), most notably those encoding cystic fibrosis transmembrane conductance regulator (*CFTR*), serine protease inhibitor Kazal type 1 (*SPINK1*), and chymotrypsin C (*CTRC*).[64–70] Sequencing analysis has determined that 40% to 50% of adults with ICP have a mutation in *PRSS1*, *SPINK1*, and/or *CFTR*, and the prevalence is as high as 79% in a pediatric cohort.[71–74] This raises the possibility that these risk loci may in fact be causative in some cases of ICP, especially when two or more loci carry mutations. Based on these epidemiologic studies and the established role of trypsinogen autoactivation in pancreatitis pathogenesis, it is believed that dysfunction of either ductal secretion or the inhibition of trypsinogen autoactivation predisposes individuals to pancreatitis. These studies employed targeted sequencing of risk loci, precluding the discovery of novel mutations in other genes; therefore, as genomewide approaches in HCP and ICP patient cohorts become more commonplace, risk loci related to ductal hypersecretion may indeed be identified and may include *HHEX*.

References

1. Matthews EK, Petersen OH, Williams JA. Pancreatic acinar cells: acetylcholine-induced membrane depolarization, calcium efflux and amylase release. J Physiol 1973;234:689–701.

2. Petersen OH, Ueda N. Pancreatic acinar cells: effect of acetylcholine, pancreozymin, gastrin and secretin on membrane potential and resistance in vivo and in vitro. J Physiol 1975;247:461–471.

3. Reichert M, Rustgi AK. Pancreatic ductal cells in development, regeneration, and neoplasia. J Clin Invest 2011;121:4572–4578.

4. Whitcomb DC, Ermentrout GB. A mathematical model of the pancreatic duct cell generating high bicarbonate concentrations in pancreatic juice. Pancreas 2004;29:e30–e40.

5. Folsch UR, Fischer H, Soling HD, et al. Effects of gastrointestinal hormones and carbamylcholine on cAMP accumulation in isolated pancreatic duct fragments from the rat. Digestion 1980;20:277–292.

6. Gray MA, Plant S, Argent BE. cAMP-regulated whole cell chloride currents in pancreatic duct cells. Am J Physiol 1993;264:C591–C602.

7. Ashton N, Argent BE, Green R. Effect of vasoactive intestinal peptide, bombesin and substance P on fluid secretion by isolated rat pancreatic ducts. J Physiol 1990;427:471–482.

8. Ashton N, Argent BE, Green R. Characteristics of fluid secretion from isolated rat pancreatic ducts stimulated with secretin and bombesin. J Physiol 1991;435:533–546.

9. Ashton N, Evans RL, Elliott AC, et al. Regulation of fluid secretion and intracellular messengers in isolated rat pancreatic ducts by acetylcholine. J Physiol 1993;471:549–562.

10. Ishiguro H, Naruse S, Kitagawa M, et al. Luminal ATP stimulates fluid and HCO_3- secretion in guinea-pig pancreatic duct. J Physiol 1999;519 Pt 2:551–558.

11. Haanes KA, Novak I. ATP storage and uptake by isolated pancreatic zymogen granules. Biochem J 2010;429:303–311.

12. Freedman SD, Scheele GA. Regulated secretory proteins in the exocrine pancreas aggregate under conditions that mimic the trans-Golgi network. Biochem Biophys Res Commun 1993;197:992–999.

13. Riordan JR, Rommens JM, Kerem B, et al. Identification of the cystic fibrosis gene: cloning and characterization of complementary DNA. Science 1989; 245:1066–1073.

14. Kopelman H, Corey M, Gaskin K, et al. Impaired chloride secretion, as well as bicarbonate secretion, underlies the fluid secretory defect in the cystic fibrosis pancreas. Gastroenterology 1988;95:349–355.

15. Raimondi S, Lowenfels AB, Morselli-Labate AM, et al. Pancreatic cancer in chronic pancreatitis; aetiology, incidence, and early detection. Best Pract Res Clin Gastroenterol 2010;24:349–358.

16. Crompton MR, Bartlett TJ, MacGregor AD, et al. Identification of a novel vertebrate homeobox gene expressed in haematopoietic cells. Nucleic Acids Res 1992; 20:5661–5667.

17. Zhang J, McKenna LB, Bogue CW, et al. The diabetes gene Hhex maintains delta-cell differentiation and islet function. Genes Dev 2014;28:829–834.

18. Guo Y, Chan R, Ramsey H, et al. The homeoprotein Hex is required for hemangioblast differentiation. Blood 2003; 102:2428–2435.

19. Hallaq H, Pinter E, Enciso J, et al. A null mutation of Hhex results in abnormal cardiac development, defective vasculogenesis and elevated Vegfa levels. Development 2004;131:5197–5209.

20. Martinez Barbera JP, Clements M, Thomas P, et al. The homeobox gene *Hex* is required in definitive endodermal tissues for normal forebrain, liver and thyroid formation. Development 2000;127:2433–2445.

21. Keng VW, Fujimori KE, Myint Z, et al. Expression of Hex mRNA in early murine postimplantation embryo development. FEBS Lett 1998;426:183–186.

22. Thomas PQ, Brown A, Beddington RS. Hex: a homeobox gene revealing peri-implantation asymmetry in the mouse embryo and an early transient marker of endothelial cell precursors. Development 1998;125:85–94.

23. Bogue CW, Ganea GR, Sturm E, et al. Hex expression suggests a role in the development and function of organs derived from foregut endoderm. Dev Dyn 2000; 219:84–89.

24. Bort R, Martinez-Barbera JP, Beddington RS, et al. *Hex* homeobox gene-dependent tissue positioning is required for organogenesis of the ventral pancreas. Development 2004;131:797–806.

25. Bort R, Signore M, Tremblay K, et al. *Hex* homeobox gene controls the transition of the endoderm to a pseudostratified, cell emergent epithelium for liver bud development. Dev Biol 2006;290:44–56.

26. Yamamoto M, Otani M, Otsuki M. A new model of chronic pancreatitis in rats. Am J Physiol Gastrointest Liver Physiol 2006;291:G700–G708.

27. Sabbatini ME, Villagra A, Davio CA, et al. Atrial natriuretic factor stimulates exocrine pancreatic secretion in the rat through NPR-C receptors. Am J Physiol Gastrointest Liver Physiol 2003;285:G929–G937.

28. Hunter MP, Wilson CM, Jiang X, et al. The homeobox gene *Hhex* is essential for proper hepatoblast differentiation and bile duct morphogenesis. Dev Biol 2007; 308:355–367.

29. Gu G, Dubauskaite J, Melton DA. Direct evidence for the pancreatic lineage: NGN3+ cells are islet progenitors and are distinct from duct progenitors. Development 2002; 129:2447–2457.

30. Kopp JL, Dubois CL, Schaffer AE, et al. Sox9+ ductal cells are multipotent progenitors throughout development but do not produce new endocrine cells in the normal or injured adult pancreas. Development 2011; 138:653–665.

31. Le Lay J, Tuteja G, White P, et al. *CRTC2 (TORC2)* contributes to the transcriptional response to fasting in the liver but is not required for the maintenance of glucose homeostasis. Cell Metab 2009;10:55–62.

32. Grant GR, Farkas MH, Pizarro AD, et al. Comparative analysis of RNA-Seq alignment algorithms and the RNA-Seq unified mapper (RUM). Bioinformatics 2011; 27:2518–2528.

33. Robinson MD, McCarthy DJ, Smyth GK. edgeR: a Bioconductor package for differential expression analysis of digital gene expression data. Bioinformatics 2010; 26:139–140.

34. Reichert M, Takano S, Heeg S, et al. Isolation, culture and genetic manipulation of mouse pancreatic ductal cells. Nat Protoc 2013;8:1354–1365.

35. Pierreux CE, Poll AV, Kemp CR, et al. The transcription factor hepatocyte nuclear factor-6 controls the development of pancreatic ducts in the mouse. Gastroenterology 2006;130:532–541.

36. Zhang H, Ables ET, Pope CF, et al. Multiple, temporal-specific roles for *HNF6* in pancreatic endocrine and ductal differentiation. Mech Dev 2009;126:958–973.

37. Gresh L, Fischer E, Reimann A, et al. A transcriptional network in polycystic kidney disease. EMBO J 2004; 23:1657–1668.

38. Cano DA, Murcia NS, Pazour GJ, et al. Orpk mouse model of polycystic kidney disease reveals essential role of primary cilia in pancreatic tissue organization. Development 2004;131:3457–3467.

39. Cano DA, Sekine S, Hebrok M. Primary cilia deletion in pancreatic epithelial cells results in cyst formation and pancreatitis. Gastroenterology 2006;131:1856–1869.

40. Prevot PP, Simion A, Grimont A, et al. Role of the ductal transcription factors *HNF6* and *Sox9* in pancreatic acinar-to-ductal metaplasia. Gut 2012;61:1723–1732.

41. Coffinier C, Barra J, Babinet C, et al. Expression of the vHNF1/HNF1beta homeoprotein gene during mouse organogenesis. Mech Dev 1999;89:211–213.

42. Kopp JL, von Figura G, Mayes E, et al. Identification of *Sox9*-dependent acinar-to-ductal reprogramming as the principal mechanism for initiation of pancreatic ductal adenocarcinoma. Cancer Cell 2012;22:737–750.

43. Asaumi H, Watanabe S, Taguchi M, et al. Externally applied pressure activates pancreatic stellate cells through the generation of intracellular reactive oxygen species. Am J Physiol Gastrointest Liver Physiol 2007; 293:G972–G978.

44. Andoh A, Takaya H, Saotome T, et al. Cytokine regulation of chemokine (IL-8, MCP-1, and RANTES) gene expression in human pancreatic periacinar myofibroblasts. Gastroenterology 2000;119:211–219.

45. Shek FW, Benyon RC, Walker FM, et al. Expression of transforming growth factor-beta 1 by pancreatic stellate cells and its implications for matrix secretion and turnover in chronic pancreatitis. Am J Pathol 2002; 160:1787–1798.

46. Jalleh RP, Aslam M, Williamson RC. Pancreatic tissue and ductal pressures in chronic pancreatitis. Br J Surg 1991;78:1235–1237.

47. de Bold AJ, Bruneau BG, Kuroski de Bold ML. Mechanical and neuroendocrine regulation of the endocrine heart. Cardiovasc Res 1996;31:7–18.

48. Brenner BM, Ballermann BJ, Gunning ME, et al. Diverse biological actions of atrial natriuretic peptide. Physiol Rev 1990;70:665–699.

49. Gower WR Jr, Dietz JR, Vesely DL, et al. Atrial natriuretic peptide gene expression in the rat gastrointestinal tract. Biochem Biophys Res Commun 1994;202:562–570.

50. Vollmar AM, Paumgartner G, Gerbes AL. Differential gene expression of the three natriuretic peptides and natriuretic peptide receptor subtypes in human liver. Gut 1997;40:145–150.

51. Gower WR Jr, Salhab KF, Foulis WL, et al. Regulation of atrial natriuretic peptide gene expression in gastric antrum by fasting. Am J Physiol Regul Integr Comp Physiol 2000;278:R770–R780.

52. Chabot JG, Morel G, Kopelman H, et al. Atrial natriuretic factor and exocrine pancreas: autoradiographic localization of binding sites and ultrastructural evidence for internalization of endogenous ANF. Pancreas 1987; 2:404–413.

53. Chabot JG, Morel G, Belles-Isles M, et al. ANF and exocrine pancreas: ultrastructural autoradiographic localization in acinar cells. Am J Physiol 1988; 254:E301–E309.

54. Rindler MJ, Xu CF, Gumper I, et al. Proteomic analysis of pancreatic zymogen granules: identification of new granule proteins. J Proteome Res 2007;6:2978–2992.

55. Hede SE, Amstrup J, Christoffersen BC, et al. Purinoceptors evoke different electrophysiological responses in pancreatic ducts. P2Y inhibits K^+ conductance, and P2X stimulates cation conductance. J Biol Chem 1999; 274:31784–31791.

56. Racz GZ, Kittel A, Riccardi D, et al. Extracellular calcium sensing receptor in human pancreatic cells. Gut 2002; 51:705–711.

57. Behrendorff N, Floetenmeyer M, Schwiening C, et al. Protons released during pancreatic acinar cell secretion acidify the lumen and contribute to pancreatitis in mice. Gastroenterology 2010;139:1711–1720, e1–5.

58. Freedman SD, Kern HF, Scheele GA. Cleavage of GPI-anchored proteins from the plasma membrane activates apical endocytosis in pancreatic acinar cells. Eur J Cell Biol 1998;75:163–173.

59. Seymour PA, Freude KK, Tran MN, et al. SOX9 is required for maintenance of the pancreatic progenitor cell pool. Proc Natl Acad Sci USA 2007;104:1865–1870.

60. Hezel AF, Gurumurthy S, Granot Z, et al. Pancreatic LKB1 deletion leads to acinar polarity defects and cystic neoplasms. Mol Cell Biol 2008;28:2414–2425.

61. Ceppa EP, Pitt HA, Hunter JL, et al. Hereditary pancreatitis: endoscopic and surgical management. J Gastrointest Surg 2013;17:847–857.

62. Rebours V, Boutron-Ruault MC, Schnee M, et al. The natural history of hereditary pancreatitis: a national series. Gut 2009;58:97–103.

63. Applebaum-Shapiro SE, Finch R, Pfutzer RH, et al. Hereditary pancreatitis in North America: the Pittsburgh-Midwest Multi-Center Pancreatic Study Group Study. Pancreatology 2001;1:439–443.

64. Whitcomb DC, Gorry MC, Preston RA, et al. Hereditary pancreatitis is caused by a mutation in the cationic trypsinogen gene. Nat Genet 1996;14:141–145.

65. Schneider A, Larusch J, Sun X, et al. Combined bicarbonate conductance-impairing variants in CFTR and SPINK1 variants are associated with chronic pancreatitis in patients without cystic fibrosis. Gastroenterology 2011;140:162–171.

66. Rosendahl J, Witt H, Szmola R, et al. Chymotrypsin C (CTRC) variants that diminish activity or secretion are associated with chronic pancreatitis. Nat Genet 2008; 40:78–82.

67. Sharer N, Schwarz M, Malone G, et al. Mutations of the cystic fibrosis gene in patients with chronic pancreatitis. N Engl J Med 1998;339:645–652.

68. Cohn JA, Friedman KJ, Noone PG, et al. Relation between mutations of the cystic fibrosis gene and idiopathic pancreatitis. N Engl J Med 1998;339:653–658.

69. Pfutzer RH, Barmada MM, Brunskill AP, et al. SPINK1/PSTI polymorphisms act as disease modifiers in familial and idiopathic chronic pancreatitis. Gastroenterology 2000;119:615–623.

70. Witt H, Luck W, Hennies HC, et al. Mutations in the gene encoding the serine protease inhibitor, Kazal type 1 are associated with chronic pancreatitis. Nat Genet 2000; 25:213–216.

71. Sultan M, Werlin S, Venkatasubramani N. Genetic prevalence and characteristics in children with recurrent pancreatitis. J Pediatr Gastroenterol Nutr 2012; 54:645–650.

72. Gasiorowska A, Talar-Wojnarowska R, Czupryniak L, et al. The prevalence of cationic trypsinogen (PRSS1) and serine protease inhibitor, Kazal type 1 (SPINK1) gene mutations in Polish patients with alcoholic and idiopathic chronic pancreatitis. Dig Dis Sci 2011; 56:894–901.

73. Joergensen MT, Brusgaard K, Cruger DG, et al. Genetic, epidemiological, and clinical aspects of hereditary pancreatitis: a population-based cohort study in Denmark. Am J Gastroenterol 2010;105: 1876–1883.

74. Keiles S, Kammesheidt A. Identification of CFTR, PRSS1, and SPINK1 mutations in 381 patients with pancreatitis. Pancreas 2006;33:221–227.

75. Ghosh B, Ganea GR, Denson LA, et al. Immunocytochemical characterization of murine Hex, a homeobox-containing protein. Pediatr Res 2000;48:634–638.

Correspondence
Address correspondence to: Klaus H. Kaestner, PhD, Department of Genetics, Institute for Diabetes, Obesity, and Metabolism, Perelman School of Medicine, University of Pennsylvania, 12–126 Translational Research Center, 3400 Civic Center Boulevard, Philadelphia, Pennsylvania 19104. e-mail: kaestner@mail.med.upenn.edu; fax: 215-573-5892.